

Decomposition of the QCD String into Dipoles and Unintegrated Gluon Distributions

A. I. Shoshi^{1,a}, F. D. Steffen^{1,b}, H.G. Dosch^{1,c}, and H. J. Pirner^{1,2,d}

¹*Institut für Theoretische Physik, Universität Heidelberg,
Philosophenweg 16 & 19, D-69120 Heidelberg, Germany*

²*Max-Planck-Institut für Kernphysik, Postfach 103980,
D-69029 Heidelberg, Germany*

Abstract

We present the perturbative and non-perturbative QCD structure of the dipole-dipole scattering amplitude in momentum space. The perturbative contribution is described by two-gluon exchange and the non-perturbative contribution by the stochastic vacuum model which leads to confinement of the quark and antiquark in the dipole via a string of color fields. This QCD string gives important non-perturbative contributions to high-energy reactions. A new structure different from the perturbative dipole factors is found in the string-string scattering amplitude. The string can be represented as an integral over stringless dipoles with a given dipole number density. This decomposition of the QCD string into dipoles allows us to calculate the unintegrated gluon distribution of hadrons and photons from the dipole-hadron and dipole-photon cross section via $|\vec{k}_\perp|$ -factorization.

Keywords: Confining String, Gluon Distribution, High-Energy Scattering, Non-Perturbative QCD, Stochastic Vacuum Model, Two-Gluon Exchange

PACS numbers: 11.80.Fv, 12.38.-t, 12.40.-y, 13.60.-r,

^ashoshi@tphys.uni-heidelberg.de

^bFrank.D.Steffen@thphys.uni-heidelberg.de

^cH.G.Dosch@thphys.uni-heidelberg.de

^dpir@tphys.uni-heidelberg.de

1 Introduction

One of the challenges in quantum chromodynamics (QCD) is the understanding of hadronic high-energy reactions. Asymptotic freedom allows perturbative calculations of hadron-hadron interactions at large momentum transfer. Computer simulations on Euclidean lattices give access to non-perturbative QCD and allow to investigate static properties of hadrons such as the hadron spectrum and confinement. Less is known about the non-perturbative structure of hadron-hadron scattering as non-perturbative methods working in Minkowski space-time are required.

In this work, we investigate the perturbative and non-perturbative QCD structure of the dipole-dipole scattering amplitude in momentum space. We use the recently presented loop-loop correlation model (LLCM) [1] which combines perturbative and non-perturbative QCD contributions and allows to compute cross sections of hadron-hadron, photon-hadron and photon-photon reactions in a unified description. The model is based on a functional integral approach developed for parton-parton scattering in the eikonal approximation [2, 3] and extended to gauge-invariant loop-loop scattering [4–6]. The S -matrix factorizes into the universal correlation of two light-like Wegner-Wilson loops and reaction-specific wave functions. The light-like Wegner-Wilson loops describe color-dipoles given by the quark and antiquark in the meson or photon and in a simplified picture by a quark and diquark in the baryon. The size and orientation of the color-dipoles in the hadrons and photons are determined by appropriate light-cone wave functions. The perturbative correlation is described by lowest order gluon exchange and the non-perturbative correlation by the stochastic vacuum model (SVM) [7]. The unitarization of both contributions obtained in the approach of Berger and Nachtmann [8] is important for ultra-high energies and non-forward scattering [1] and is not discussed here.

The SVM gives confinement for non-Abelian gauge theories due to flux-tube formation of color fields between the quark and antiquark of a dipole [9–11]. This flux-tube or *string* enters via the essential SVM assumption that non-perturbative interactions are most adequately described in terms of correlators of gluon field strengths instead of gluon potentials as in perturbative QCD. Therefore, the line integrals over the gluon potentials in the Wegner-Wilson loops of the functional integral approach [2–6] are transformed into surface integrals over gluon field strengths using the non-Abelian Stokes theorem [3, 12]. In line with our recent work [1] we use *minimal surfaces*, planar surfaces bounded by Wegner-Wilson loops, which are usually used to obtain Wilson’s area law in Euclidean space-time [7, 11]. Minimal surfaces allow us to show for the first time the non-perturbative structure of the dipole-dipole scattering amplitude in momentum space. The previous pyramid mantle choice for the surfaces [5, 8, 13–18] did not allow such an analysis.

The perturbative contribution to dipole-dipole scattering in our approach is the known two-gluon exchange [19, 20] between the two dipoles. The non-perturbative contribution comes out as a sum of two parts: The first part describes the non-perturbative interaction between the quarks and antiquarks of the two dipoles and exhibits the same dipole factors as the perturbative contribution. The second part represents the interaction between the strings of the two dipoles. It shows a new structure different from the perturbative two-gluon exchange. Nevertheless, we would like to emphasize that $|\vec{k}_\perp|$ -factorization is valid also for the non-perturbative contribution.

The string confining the quark-antiquark dipole of length $|\vec{r}_D|$ has an integral representation which sums stringless dipoles of sizes $\xi|\vec{r}_D|$ with $0 \leq \xi \leq 1$ and dipole number density $n(\xi) = 1/\xi^2$. Consequently, the string-hadron scattering reduces to an incoherent superposition of dipole-hadron scattering processes. This decomposition of the string into stringless dipoles allows us to extract the microscopic structure of the unintegrated gluon distribution of hadrons and photons, $\mathcal{F}_h(x, k_\perp^2)$, from our dipole-hadron and dipole-photon cross section via $|\vec{k}_\perp|$ -factorization.

The unintegrated gluon distribution of hadrons and photons $\mathcal{F}_h(x, k_\perp^2)$ is a basic, universal quantity convenient for the computation of many scattering observables at small x . It is crucial to describe processes in which transverse momenta are explicitly exposed such as dijet [21] or vector meson [22] production at HERA. Its explicit $|\vec{k}_\perp|$ -dependence is particularly suited to study the interplay between soft and hard physics. Moreover, the unintegrated gluon distribution is the central object in the BFKL [23] and CCFM [24] evolution equations. Upon integration over the transverse gluon momentum $|\vec{k}_\perp|$ it leads to the conventional gluon distribution $xG_h(x, Q^2)$ used in the DGLAP evolution equation [25].

The outline of the paper is as follows: In Sec. 2, we review the loop-loop correlation model [1] and give the model parameters. In Sec. 3, we investigate the perturbative and non-perturbative structure of the dipole-dipole scattering amplitude in momentum space. In Sec. 4, we present the decomposition of the string into dipoles, elaborate the total dipole-hadron cross section, and extract the unintegrated gluon distribution. Numerical results for the unintegrated gluon distribution of protons, pions, kaons, and photons are given in Sec. 5 together with the integrated gluon distribution of the proton $xG_p(x, Q^2)$. In Sec. 6, we compare our results for the unintegrated gluon distribution of the proton with those obtained in other approaches. We close with a summary of our results.

2 The Loop-Loop Correlation Model

Recently, we have presented a loop-loop correlation model to compute high-energy hadron-hadron, photon-hadron, and photon-photon reactions [1]. Based on the functional integral approach to high-energy scattering in the eikonal approximation [2–6], the T -matrix element for the elastic scattering of two particles 1 and 2 at transverse momentum transfer \vec{q}_\perp ($t = -\vec{q}_\perp^2$) and c.m. energy squared s reads

$$T(s, t) = 2is \int d^2b_\perp e^{i\vec{q}_\perp \vec{b}_\perp} \int dz_1 d^2r_1 \int dz_2 d^2r_2 \times |\psi_1(z_1, \vec{r}_1)|^2 |\psi_2(z_2, \vec{r}_2)|^2 \left[1 - S_{DD}(\vec{b}_\perp, z_1, \vec{r}_1, z_2, \vec{r}_2) \right], \quad (2.1)$$

where the correlation of two light-like Wegner-Wilson loops, the *loop-loop correlation function*,⁵

$$S_{DD}(\vec{b}_\perp, z_1, \vec{r}_1, z_2, \vec{r}_2) = \left\langle W[C_1]W[C_2] \right\rangle_G, \quad (2.2)$$

describes the elastic scattering of two color-dipoles (DD). The path of each color-dipole is represented by a light-like Wegner-Wilson loop [26] in the fundamental representation of $SU(3)$

$$W[C_i] = \frac{1}{3} \text{Tr} \mathcal{P} \exp \left[-ig \oint_{C_i} dz^\mu \mathcal{G}_\mu(z) \right], \quad (2.3)$$

where Tr is the trace in color space, g the strong coupling, and $\mathcal{G}_\mu(z) = \mathcal{G}_\mu^a(z)t^a$ the gluon field with the $SU(3)$ group generators t^a that demand the path ordering indicated by \mathcal{P} . Physically, the Wegner-Wilson loops (2.3) represent the phase that quarks and antiquarks acquire along the light-like trajectories C_i in the gluon background field. The color-dipoles have transverse size and orientation \vec{r}_i . The longitudinal momentum fraction of dipole i carried by the quark is z_i . The impact parameter between the dipoles is [14]

$$\vec{b}_\perp = \vec{r}_{1q} + (1 - z_1)\vec{r}_1 - \vec{r}_{2q} - (1 - z_2)\vec{r}_2 = \vec{r}_{1cm} - \vec{r}_{2cm}, \quad (2.4)$$

where \vec{r}_{iq} ($\vec{r}_{i\bar{q}}$) is the transverse position of the quark (antiquark), $\vec{r}_i = \vec{r}_{i\bar{q}} - \vec{r}_{iq}$, and $\vec{r}_{icm} = z_i\vec{r}_{iq} + (1 - z_i)\vec{r}_{i\bar{q}}$ is the center of light-cone momenta. Figure 1 illustrates the (a) space-time and (b) transverse arrangement of the loops. The QCD vacuum expectation value $\langle \dots \rangle_G$ in the loop-loop correlation function (2.2) represents functional integrals [3] in which the functional integration over the fermion fields has already been carried out as indicated by the subscript G . The model we use for the

⁵More generally, $S_{DD} = \langle W[C_1]W[C_2] \rangle_G / (\langle W[C_1] \rangle_G \langle W[C_2] \rangle_G)$. For light-like Wegner-Wilson loops, however, one obtains $\langle W[C_{1,2}] \rangle_G = 1$ as shown explicitly in [3].

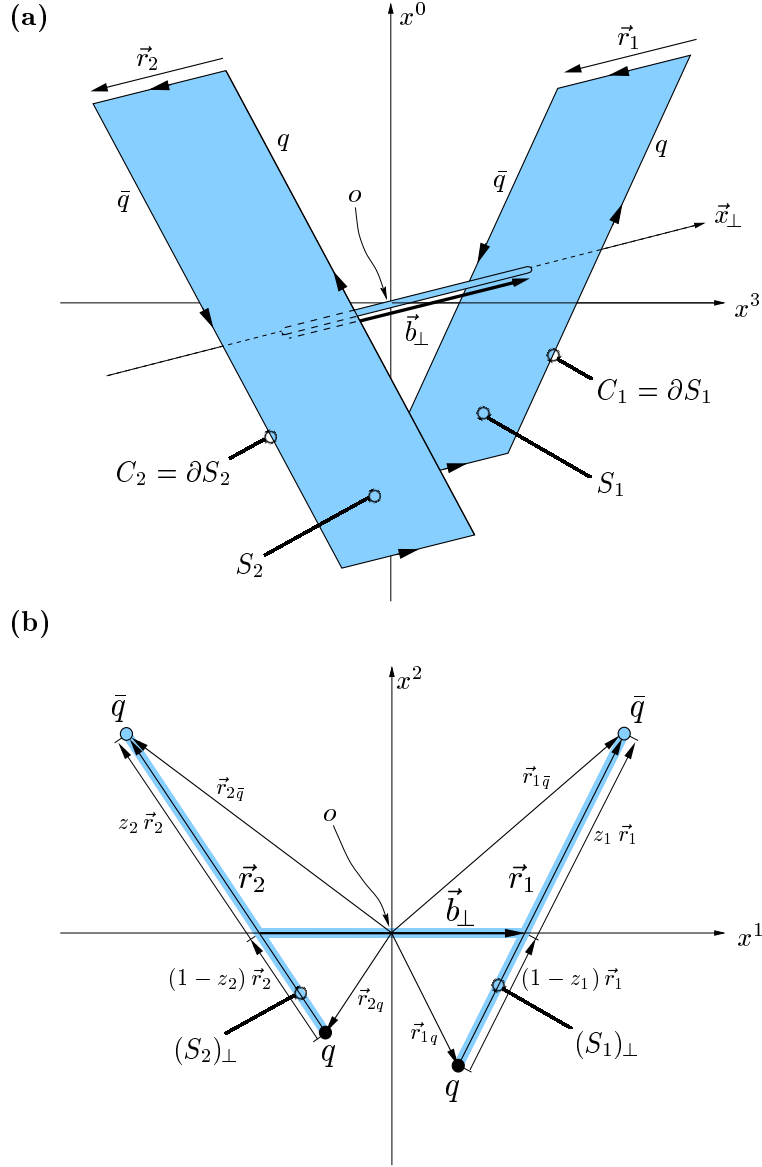


Figure 1: High-energy dipole-dipole scattering in the eikonal approximation represented by Wegner-Wilson loops: (a) space-time and (b) transverse arrangement of the Wegner-Wilson loops. The shaded areas represent the strings extending from the quark to the antiquark path in each color dipole. The thin tube allows to compare the field strengths in surface S_1 with the field strengths in surface S_2 . The impact parameter \vec{b}_\perp connects the centers of light-cone momenta of the dipoles.

QCD vacuum describes only gluon dynamics and, thus, implies the quenched approximation that does not allow string breaking through dynamical quark-antiquark production.

The \vec{r}_i and z_i distribution of the color-dipoles is given by the *wave functions* ψ_i that characterize the interacting particles. In this framework, the color-dipoles are given by the quark and antiquark in the meson or photon and in a simplified picture by a quark and diquark in the baryon. We use for hadrons the phenomenological Gaussian wave function [18, 27] and for photons the perturbatively derived wave functions with running quark masses $m_f(Q^2)$ to account for the non-perturbative region of low photon virtuality Q^2 [15] as discussed explicitly in Appendix A.

The computation of the loop-loop correlation function (2.2) in the matrix cumulant approach of Berger and Nachtmann [8] has been reviewed in detail in [1]. The main steps of this computation are the transformation of the line integrals into surface integrals with the non-Abelian Stokes theorem, a matrix cumulant expansion, and the Gaussian approximation of the functional integrals. In line with other two-component (soft + hard) models [16, 17, 28–30] and the different hadronization mechanisms in soft and hard collisions, we have further demanded that the perturbative and non-perturbative contributions do not mix on the amplitude level [1]. The resulting T -matrix element at the reference c.m. energy $\sqrt{s_0}$ reads

$$T(s_0, t) = 2is_0 \int d^2b_\perp e^{i\vec{q}_\perp \vec{b}_\perp} \int dz_1 d^2r_1 \int dz_2 d^2r_2 |\psi_1(z_1, \vec{r}_1)|^2 |\psi_2(z_2, \vec{r}_2)|^2 \times \left[1 - \frac{2}{3} \cos\left(\frac{1}{3}\chi^P\right) \cos\left(\frac{1}{3}\chi^{NP}\right) - \frac{1}{3} \cos\left(\frac{2}{3}\chi^P\right) \cos\left(\frac{2}{3}\chi^{NP}\right) \right], \quad (2.5)$$

where the arguments of the functions $\chi^{P, NP}(\vec{b}_\perp, z_1, \vec{r}_1, z_2, \vec{r}_2)$ are suppressed to lighten notation. The χ -functions defined as

$$\chi^{P, NP} := -i \frac{\pi^2}{4} \int_{S_1} d\sigma^{\mu\nu}(x_1) \int_{S_2} d\sigma^{\rho\sigma}(x_2) F_{\mu\nu\rho\sigma}^{P, NP}(x_1, x_2, o; C_{x_1o}, C_{x_2o}) \quad (2.6)$$

represent integrals over the *minimal surfaces* $S_{1,2}$ that are built from the areas spanned by the quark and antiquark paths $C_{1,2}$ of the interacting dipoles and the infinitesimally thin tube which connects the surfaces S_1 and S_2 as shown in Fig. 1. The integrand $F_{\mu\nu\rho\sigma}^{P, NP}$ is the gauge-invariant bilocal gluon field strength correlator

$$\left\langle \frac{g^2}{4\pi^2} \mathcal{G}_{\mu\nu}^a(o, x_1; C_{x_1o}) \mathcal{G}_{\rho\sigma}^b(o, x_2; C_{x_2o}) \right\rangle_G^{P, NP} =: \frac{1}{4} \delta^{ab} F_{\mu\nu\rho\sigma}^{P, NP}(x_1, x_2, o; C_{x_1o}, C_{x_2o}), \quad (2.7)$$

where the gluon field strengths $\mathcal{G}_{\mu\nu}(x_i)$ are parallel transported to the common reference point o along the path $C_{x_i o}$

$$\mathcal{G}_{\mu\nu}(o, x_i; C_{x_i o}) = \Phi(x_i, o; C_{x_i o})^{-1} \mathcal{G}_{\mu\nu}(x_i) \Phi(x, o; C_{x_i o}) \quad (2.8)$$

with the QCD Schwinger string

$$\Phi(x_i, o; C_{x_i o}) = \mathcal{P} \exp \left[-ig \int_{C_{x_i o}} dz^\mu \mathcal{G}_\mu(z) \right] \quad (2.9)$$

to ensure gauge invariance in the model. In (2.7), $F_{\mu\nu\rho\sigma}^P$ gives the perturbative (P) physics (short-range correlations) described by *perturbative gluon exchange* and $F_{\mu\nu\rho\sigma}^{NP}$ the non-perturbative (NP) physics (long-range correlations) modelled by the *stochastic vacuum model* (SVM) [7].

In leading order in the strong coupling g , the perturbative bilocal gluon field strength correlator $F_{\mu\nu\rho\sigma}^P$ is gauge-invariant already without the parallel transport to a common reference point and depends only on the difference $z := x_1 - x_2$,

$$\begin{aligned} F_{\mu\nu\rho\sigma}^P(z) &= \frac{g^2}{\pi^2} \frac{1}{2} \left[\frac{\partial}{\partial z_\nu} (z_\sigma g_{\mu\rho} - z_\rho g_{\mu\sigma}) + \frac{\partial}{\partial z_\mu} (z_\rho g_{\nu\sigma} - z_\sigma g_{\nu\rho}) \right] D_P(z^2) \\ &= -\frac{g^2}{\pi^2} \int \frac{d^4 k}{(2\pi)^4} e^{-ikz} \left[k_\nu k_\sigma g_{\mu\rho} - k_\nu k_\rho g_{\mu\sigma} + k_\mu k_\rho g_{\nu\sigma} - k_\mu k_\sigma g_{\nu\rho} \right] \tilde{D}'_P(k^2). \end{aligned} \quad (2.10)$$

Here, we have introduced an effective gluon mass $m_G = m_\rho = 0.77 \text{ GeV}$ as infrared regulator in the perturbative correlation function

$$\tilde{D}'_P(k^2) := \frac{d}{dk^2} \int d^4 z D_P(z^2) e^{ikz} = \frac{i}{k^2 - m_G^2}, \quad (2.11)$$

and a parameter $M^2 = 1.04 \text{ GeV}^2$ which freezes the running coupling⁶ in the quenched approximation at the value $\alpha_s(k_\perp^2 = 0) = 0.4$ [11],

$$\alpha_s(k_\perp^2) = \frac{g^2(k_\perp^2)}{4\pi} = \frac{1}{11 \ln [(k_\perp^2 + M^2)/\Lambda_{QCD}^2]}. \quad (2.12)$$

If the path connecting the points x_1 and x_2 is a straight line, the non-perturbative correlator $F_{\mu\nu\rho\sigma}^{NP}$ depends also only on the difference $z := x_1 - x_2$. Then, the most general form of the correlator in four-dimensional Minkowski space-time that respects

⁶Only the running coupling as a function of the transverse momentum is needed in the final result.

translational, Lorentz, and parity invariance reads [4–6]

$$F_{\mu\nu\rho\sigma}^{NP}(z) := F_{\mu\nu\rho\sigma}^{NP(nc)}(z) + F_{\mu\nu\rho\sigma}^{NP(c)}(z) \quad (2.13)$$

$$\begin{aligned} F_{\mu\nu\rho\sigma}^{NP(nc)}(z) &= \frac{G_2(1-\kappa)}{6(N_c^2-1)} \left(\frac{\partial}{\partial z_\nu} (z_\sigma g_{\mu\rho} - z_\rho g_{\mu\sigma}) + \frac{\partial}{\partial z_\mu} (z_\rho g_{\nu\sigma} - z_\sigma g_{\nu\rho}) \right) D_1(z^2) \\ &= -\frac{G_2(1-\kappa)}{6(N_c^2-1)} \int \frac{d^4k}{(2\pi)^4} e^{-ikz} \left(k_\nu k_\sigma g_{\mu\rho} - k_\nu k_\rho g_{\mu\sigma} + k_\mu k_\rho g_{\nu\sigma} - k_\mu k_\sigma g_{\nu\rho} \right) \tilde{D}'_1(k^2) \end{aligned} \quad (2.14)$$

$$\begin{aligned} F_{\mu\nu\rho\sigma}^{NP(c)}(z) &= \frac{G_2\kappa}{3(N_c^2-1)} (g_{\mu\rho}g_{\nu\sigma} - g_{\mu\sigma}g_{\nu\rho}) D(z^2) \\ &= \frac{G_2\kappa}{3(N_c^2-1)} (g_{\mu\rho}g_{\nu\sigma} - g_{\mu\sigma}g_{\nu\rho}) \int \frac{d^4k}{(2\pi)^4} e^{-ikz} \tilde{D}(k^2) \end{aligned} \quad (2.15)$$

and was originally constructed in Euclidean space-time [7]. In all previous applications of the SVM, this form depending only on x_1 and x_2 has been used. New lattice results on the path dependence of the correlator [31] show a dominance of the shortest path. This result is effectively incorporated in the model since the straight paths dominate in the average over all paths.

In (2.13), D_1 and D are the non-perturbative correlation functions in four-dimensional Minkowski space-time and

$$\tilde{D}'_1(k^2) := \frac{d}{dk^2} \int d^4z D_1(z^2) e^{ikz} . \quad (2.16)$$

The Minkowskian correlation functions D_1 and D are derived [1] from the simple *exponential correlation functions* in four-dimensional Euclidean space-time

$$D_1^E(Z^2) = D^E(Z^2) = \exp(-|Z|/a) , \quad (2.17)$$

that are motivated by lattice QCD measurements of the gluon field strength correlator $F_{\mu\nu\rho\sigma}^{NP}(Z)$ [32, 33]. The parameters are the correlation length $a = 0.302$ fm, the gluon condensate $G_2 := \langle \frac{g^2}{4\pi^2} \mathcal{G}_{\mu\nu}^a(0) \mathcal{G}_{\mu\nu}^a(0) \rangle = 0.074 \text{ GeV}^4$, and the relative weight of the two different tensor structures $\kappa = 0.74$.

The correlator (2.13) is a sum of the two different tensor structures $F_{\mu\nu\rho\sigma}^{NP(nc)}(z)$ and $F_{\mu\nu\rho\sigma}^{NP(c)}(z)$. The first (2.14) is characteristic for Abelian gauge theories and does not lead to confinement, while the second (2.15) can only occur in non-Abelian gauge theories and Abelian gauge-theories with monopoles and leads to confinement when considered in Euclidean space-time [7]. Therefore, we call the tensor structure multiplied by $(1-\kappa)$ non-confining (*nc*) and the one multiplied by κ confining (*c*).

With the correlators (2.11) and (2.13) and the minimal surfaces shown in Fig. 1, the functions χ^P and $\chi^{NP} = \chi_{nc}^{NP} + \chi_c^{NP}$ have the following form [1]

$$\chi^P = 4\pi \int \frac{d^2 k_\perp}{(2\pi)^2} \alpha_s(k_\perp^2) i\tilde{D}'^{(2)}(k_\perp^2) \left[e^{i\vec{k}_\perp(\vec{r}_{1q}-\vec{r}_{2q})} + e^{i\vec{k}_\perp(\vec{r}_{1\bar{q}}-\vec{r}_{2\bar{q}})} - e^{i\vec{k}_\perp(\vec{r}_{1q}-\vec{r}_{2\bar{q}})} - e^{i\vec{k}_\perp(\vec{r}_{1\bar{q}}-\vec{r}_{2q})} \right] \quad (2.18)$$

$$\chi_{nc}^{NP} = \frac{\pi^2 G_2 (1 - \kappa)}{24} \int \frac{d^2 k_\perp}{(2\pi)^2} i\tilde{D}'^{(2)}(k_\perp^2) \left[e^{i\vec{k}_\perp(\vec{r}_{1q}-\vec{r}_{2q})} + e^{i\vec{k}_\perp(\vec{r}_{1\bar{q}}-\vec{r}_{2\bar{q}})} - e^{i\vec{k}_\perp(\vec{r}_{1q}-\vec{r}_{2\bar{q}})} - e^{i\vec{k}_\perp(\vec{r}_{1\bar{q}}-\vec{r}_{2q})} \right] \quad (2.19)$$

$$\chi_c^{NP} = \frac{\pi^2 G_2 \kappa}{24} (\vec{r}_1 \cdot \vec{r}_2) \int_0^1 dv_1 \int_0^1 dv_2 \int \frac{d^2 k_\perp}{(2\pi)^2} i\tilde{D}^{(2)}(k_\perp^2) e^{i\vec{k}_\perp(\vec{r}_{1q}+v_1\vec{r}_1-\vec{r}_{2q}-v_2\vec{r}_2)} , \quad (2.20)$$

where $\tilde{D}'^{(2)}(k_\perp^2)$, $\tilde{D}'^{(2)}(k_\perp^2)$ and $\tilde{D}^{(2)}(k_\perp^2)$ are the Minkowskian correlation functions in transverse space obtained from (2.11) and (2.17),

$$i\tilde{D}'^{(2)}(k_\perp^2) = \frac{1}{k_\perp^2 + m_G^2} , \quad (2.21)$$

$$i\tilde{D}'^{(2)}(k_\perp^2) = \frac{30 \pi^2}{a(k_\perp^2 + a^{-2})^{\frac{7}{2}}} , \quad (2.22)$$

$$i\tilde{D}^{(2)}(k_\perp^2) = \frac{12 \pi^2}{a(k_\perp^2 + a^{-2})^{\frac{5}{2}}} . \quad (2.23)$$

The component χ^P describes the perturbative interaction of the quark and antiquark of one dipole with the quark and antiquark of the other dipole as evident from the \vec{r}_{iq} and $\vec{r}_{i\bar{q}}$ dependence of (2.18) and Fig. 1b. The component χ_{nc}^{NP} has the same structure as χ^P and gives the non-perturbative interaction between the quarks and antiquarks of the dipoles. With the term quark used genuinely for quarks and antiquarks in the following, we refer to χ^P and χ_{nc}^{NP} as *quark-quark interactions*.

The component χ_c^{NP} given in (2.20) shows a different structure. Here, the integrations over v_1 and v_2 sum non-perturbative interactions between the gluon field strengths connecting the quark and antiquark in each of the two dipoles. These connections are manifestations of the strings that confine the corresponding quark and antiquark in the dipole and are visualized in Fig. 1b. Indeed, the SVM shows a flux tube between a static quark-antiquark pair in Euclidean space-time [9–11]. Therefore, we understand the confining component χ_c^{NP} as a *string-string interaction*.

The mixed contribution $\chi_{nc}^{NP} \chi_c^{NP}$ that occurs in cross sections discussed in the next sections gives the non-perturbative interaction of the quark and antiquark of one dipole with the string of the other dipole, i.e., it represents the *quark-string interaction*.

In our previous paper [1], we studied extensively the phenomenological performance of the model. With a strong and weak powerlike energy dependence ascribed respectively to χ^P and χ^{NP} , we have achieved a successful description of many different observables for hadron-hadron, proton-photon and photon-photon reactions over a wide energy range. Therefore, we adopt from [1] all given parameter values. The phenomenological energy dependence, however, is not essential for the structural aspects discussed in this work. Observables obtained with the T -matrix element (2.5) agree with experimental data at a fixed c.m. energy of $\sqrt{s_0} \approx 20$ GeV.

In this paper, we focus on the analytic structure of the model and concentrate on the limit of small χ -functions, $\chi^P < 1$ and $\chi^{NP} < 1$, in which the T -matrix element (2.5) simplifies to the sum of a perturbative (P) and non-perturbative (NP) component

$$\begin{aligned}
T(s_0, t) &= 2is_0 \int d^2b_\perp e^{i\vec{a}_\perp \vec{b}_\perp} \int dz_1 d^2r_1 \int dz_2 d^2r_2 |\psi_1(z_1, \vec{r}_1)|^2 |\psi_2(z_2, \vec{r}_2)|^2 \\
&\times \frac{1}{9} \left[(\chi^P)^2 + (\chi^{NP})^2 \right].
\end{aligned}
\tag{2.24}$$

We show in the next section that the perturbative component, $(\chi^P)^2$, describes *two-gluon exchange* [19, 20] and that the non-perturbative component, $(\chi^{NP})^2$, represents the corresponding non-perturbative two-point interaction. The main motivation of this paper is to calculate the analytic structure of this non-perturbative interaction in momentum space.

3 The Structure of Dipole-Dipole Scattering in Momentum Space

In this section, we calculate the perturbative and non-perturbative QCD contribution to the dipole-dipole (DD) scattering amplitude in momentum space. Beyond the known perturbative two-gluon-exchange interaction between the dipoles [19, 20] new insights into the non-perturbative structure of the scattering process are obtained within the SVM. The non-perturbative string-string interactions show a new structure different from the dipole factors of the perturbative contribution.

The total dipole-dipole cross section in the small- χ limit is obtained from (2.24) via the optical theorem

$$\begin{aligned}\sigma_{DD}^{tot}(s_0) &= \frac{1}{s_0} \text{Im} T(s_0, t=0) \\ &= 2 \int d^2 b_\perp \int dz_1 d^2 r_1 \int dz_2 d^2 r_2 |\psi_{D_1}(z_1, \vec{r}_1)|^2 |\psi_{D_2}(z_2, \vec{r}_2)|^2 \\ &\quad \times \frac{1}{9} \left[(\chi^P)^2 + (\chi_{nc}^{NP} + \chi_c^{NP})^2 \right],\end{aligned}\quad (3.1)$$

where the dipoles have fixed z_i and $|\vec{r}_i|$ values but are averaged over all orientations

$$|\psi_{D_i}(z_i, \vec{r}_i)|^2 = \frac{1}{2\pi |\vec{r}_{D_i}|} \delta(|\vec{r}_i| - |\vec{r}_{D_i}|) \delta(z_i - z_{D_i}). \quad (3.2)$$

All integrations in (3.1) can be carried out analytically except the one over transverse momentum $|\vec{k}_\perp|$ that enters through the χ -functions (2.18)–(2.20). The perturbative (P) and non-perturbative (NP) integrand of the resulting total dipole-dipole cross section

$$\sigma_{DD}^{tot}(s_0) = \int d|\vec{k}_\perp| \left[I^P(s_0, |\vec{k}_\perp|) + I^{NP}(s_0, |\vec{k}_\perp|) \right] \quad (3.3)$$

$$= \int d|\vec{k}_\perp| \left[I^P(s_0, |\vec{k}_\perp|) + I_{qq}^{NP}(s_0, |\vec{k}_\perp|) + I_{ss}^{NP}(s_0, |\vec{k}_\perp|) \right], \quad (3.4)$$

show the following momentum-space structure

$$\begin{aligned}I^P(s_0, |\vec{k}_\perp|) &= \frac{2}{9} \frac{1}{2\pi} |\vec{k}_\perp| (4\pi\alpha_s(k_\perp^2))^2 \left[i\tilde{D}'^{(2)}(k_\perp^2) \right]^2 \\ &\quad \times \left[2 \langle \psi_{D_1} | 1 - e^{i\vec{k}_\perp \vec{r}_1} | \psi_{D_1} \rangle 2 \langle \psi_{D_2} | 1 - e^{i\vec{k}_\perp \vec{r}_2} | \psi_{D_2} \rangle \right]\end{aligned}\quad (3.5)$$

$$\begin{aligned}I_{qq}^{NP}(s_0, |\vec{k}_\perp|) &= \frac{2}{9} \frac{1}{2\pi} |\vec{k}_\perp| \left(\frac{\pi^2 G_2}{24} \right)^2 \left[(1 - \kappa) i\tilde{D}_1^{(2)}(k_\perp^2) + \frac{\kappa}{k_\perp^2} i\tilde{D}^{(2)}(k_\perp^2) \right]^2 \\ &\quad \times \left[2 \langle \psi_{D_1} | 1 - e^{i\vec{k}_\perp \vec{r}_1} | \psi_{D_1} \rangle 2 \langle \psi_{D_2} | 1 - e^{i\vec{k}_\perp \vec{r}_2} | \psi_{D_2} \rangle \right]\end{aligned}\quad (3.6)$$

$$\begin{aligned}I_{ss}^{NP}(s_0, |\vec{k}_\perp|) &= \frac{2}{9} \frac{1}{2\pi} |\vec{k}_\perp| \left(\frac{\pi^2 G_2}{24} \right)^2 \left[\frac{\kappa}{k_\perp^2} i\tilde{D}^{(2)}(k_\perp^2) \right]^2 \\ &\quad \times \left[2 \langle \psi_{D_1} | \tan^2 \phi_1 (1 - e^{i\vec{k}_\perp \vec{r}_1}) | \psi_{D_1} \rangle 2 \langle \psi_{D_2} | \tan^2 \phi_2 (1 - e^{i\vec{k}_\perp \vec{r}_2}) | \psi_{D_2} \rangle \right]\end{aligned}\quad (3.7)$$

where the brackets $\langle \psi_{D_i} | \dots | \psi_{D_i} \rangle$ denote the averages

$$\langle \psi_{D_i} | A_i | \psi_{D_i} \rangle = \int dz_i d^2 r_i |\psi_{D_i}(z_i, \vec{r}_i)|^2 A_i \quad (3.8)$$

and the dipole orientation ϕ_i is defined as the angle between transverse momentum \vec{k}_\perp and dipole vector \vec{r}_i . With (3.2) the integration over the dipole orientations ϕ_i leads respectively to the Bessel function $J_0(|\vec{k}_\perp||\vec{r}_{D_i}|)$ and the generalized hypergeometric function⁷ ${}_1F_2(-1/2; 1/2, 1; -k_\perp^2 r_{D_i}^2/4)$

$$\begin{aligned} \langle \psi_{D_i} | 1 - e^{i\vec{k}_\perp \vec{r}_i} | \psi_{D_i} \rangle &= \frac{1}{2\pi} \int_0^{2\pi} d\phi_i (1 - e^{i\vec{k}_\perp \vec{r}_{D_i}}) \\ &= 1 - J_0(|\vec{k}_\perp||\vec{r}_{D_i}|) , \end{aligned} \quad (3.9)$$

$$\begin{aligned} \langle \psi_{D_i} | \tan^2 \phi_i (1 - e^{i\vec{k}_\perp \vec{r}_i}) | \psi_{D_i} \rangle &= \frac{1}{2\pi} \int_0^{2\pi} d\phi_i \tan^2 \phi_i (1 - e^{i\vec{k}_\perp \vec{r}_{D_i}}) \\ &= -1 + {}_1F_2\left(-\frac{1}{2}; \frac{1}{2}, 1; -\frac{k_\perp^2 r_{D_i}^2}{4}\right) . \end{aligned} \quad (3.10)$$

The important implications will be discussed in the next section.

The integrand I^P given in (3.5) describes the known perturbative two-gluon⁸ exchange [19, 20] between the quarks and antiquarks of the two dipoles. The ingredients of I^P are visualized for one combination of gluon exchanges in Fig. 2a: the paired horizontal lines represent the *dipole factors* $(1 - e^{i\vec{k}_\perp \vec{r}_i})$ that describe the phase difference between the quark and antiquark at separate transverse positions, the surrounding brackets indicate the average over the dipole orientations (3.8), the two curly lines illustrate the gluon propagator squared $[i\tilde{D}'^{(2)}]^2$, and the four vertices (dots) correspond to the strong coupling to the fourth power $g^4 = (4\pi\alpha_s)^2$.

The integrand $I^{NP} = I_{qq}^{NP} + I_{ss}^{NP}$ given in (3.6) and (3.7) describes the non-perturbative interactions: the quark-quark, string-string, and quark-string interactions identified by the appropriate correlation functions $[i\tilde{D}'^{(2)}]^2$, $[i\tilde{D}^{(2)}]^2$, and $[i\tilde{D}'^{(2)} i\tilde{D}^{(2)}]$. These interactions are illustrated in Figs. 2b, 2c and 2d, respectively. Analogous to the perturbative interaction in Fig. 2a, the dashed and solid zig-zag lines represent respectively the non-confining $(1 - \kappa) i\tilde{D}'^{(2)}$ and the confining $(\kappa/k_\perp^2) i\tilde{D}^{(2)}$ non-perturbative correlations, the shaded areas symbolize the strings, and the four vertices (squares) in each figure indicate the "non-perturbative coupling" to the fourth power $g_{NP}^4 := (\pi^2 G_2/24)^2$.

The integrand I_{qq}^{NP} describes the non-perturbative *interactions between the quarks and antiquarks* of the two dipoles and exhibits the same dipole factors $(1 - e^{i\vec{k}_\perp \vec{r}_i})$ that

⁷A review of generalized hypergeometric functions can be found in [34]. In the computer program Mathematica [35] "HypergeometricPFQ[{-1/2}, {1/2, 1}, -k_\perp^2 r_D^2/4]" denotes this function.

⁸The exact T -matrix element (2.5) important to describe scattering processes at ultra-high energies [1] goes beyond two-gluon exchange due to the higher orders in the cosine expansion.

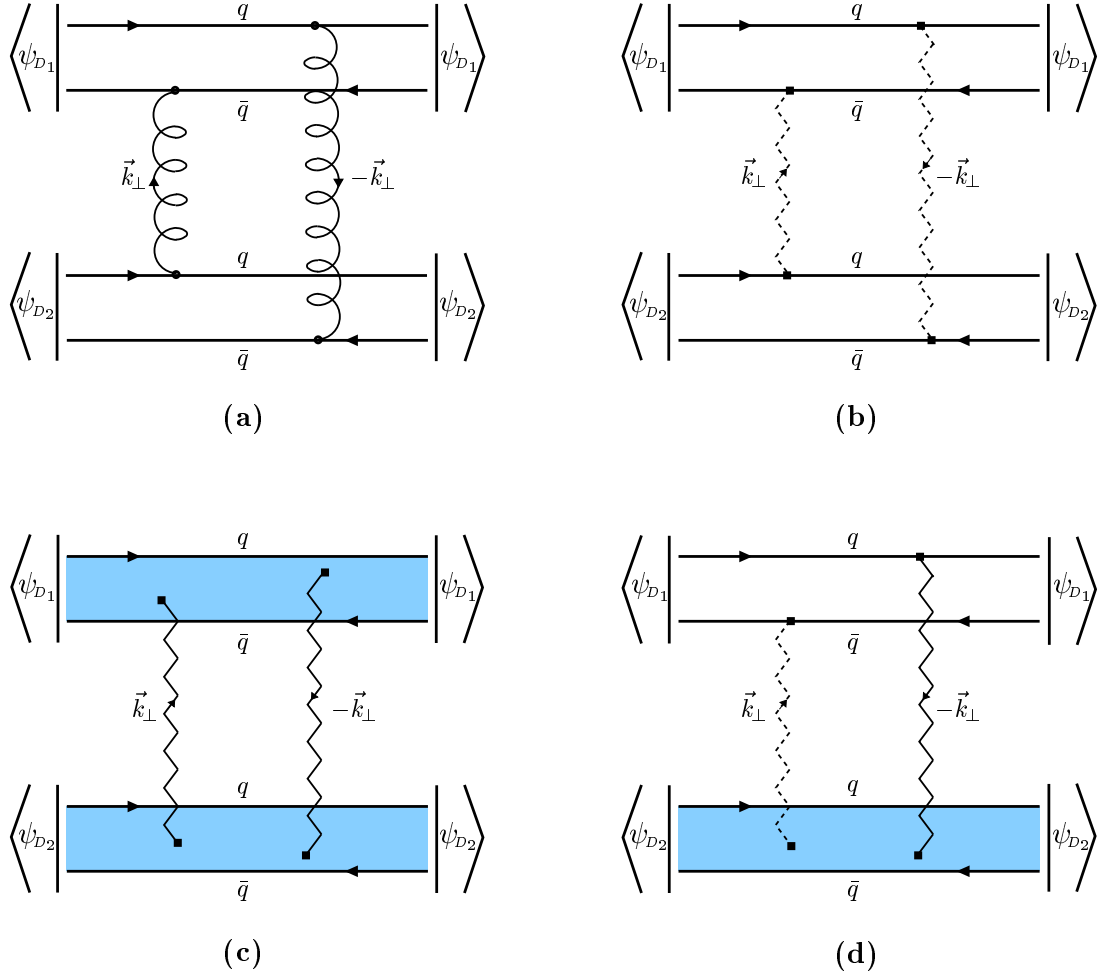


Figure 2: Perturbative and non-perturbative contributions to dipole-dipole scattering: **(a)** perturbative quark-quark interaction and non-perturbative **(b)** quark-quark, **(c)** string-string, and **(d)** quark-string interactions. The term quark is used genuinely for quarks and antiquarks. Only one diagram is shown for each type of interaction. Paired horizontal lines represent quark-antiquark dipoles, surrounding brackets indicate the averages over the dipole orientations (3.8), shaded areas visualize strings, curly lines denote exchanged perturbative gluons, and dashed and solid zig-zag lines symbolize respectively the non-perturbative non-confining and confining correlation functions.

appear in the perturbative integrand (3.5). I_{qq}^{NP} contains three components: the non-confining component, the confining component, and their interference term. While the non-confining component visualized in Fig. 2b has the same structure as the perturbative contribution, see also (2.18) and (2.19), the confining component shown in its more general form in Fig. 2c comes from the interaction between the quarks

and antiquarks at the endpoints of the strings, which will be further discussed below Eq. (3.11). The interference term describes the quark-string interaction as illustrated in Fig. 2d. Note that it reduces entirely to an interaction between the quarks and antiquarks of the dipoles with the additional denominator $1/k_{\perp}^2$ generated by the integrations over the variables v_1 and v_2 in the confining component χ_c^{NP} (2.20).

The integrand I_{ss}^{NP} describes the non-perturbative *string-string interaction* shown in Fig. 2c. The new angular dependencies in the string-string interaction, the modified dipole factors $\tan^2\phi_i(1 - e^{i\vec{k}_{\perp}\vec{r}_{D_i}})$ in (3.7), are obtained as follows. The integrations over $v_1, v_2, v'_1,$ and v'_2 in $(\chi_c^{NP})^2$ produce the dipole factors $(1 - e^{i\vec{k}_{\perp}\vec{r}_i})$ and the denominator $1/((\vec{k}_{\perp}\vec{r}_1)^2(\vec{k}_{\perp}\vec{r}_2)^2)$. This denominator multiplied with the additional factor $(\vec{r}_1\vec{r}_2)^2$ from $(\chi_c^{NP})^2$, see (2.20), gives the total angular dependence

$$\begin{aligned} \frac{(\vec{r}_1\vec{r}_2)^2}{(\vec{k}_{\perp}\vec{r}_1)^2(\vec{k}_{\perp}\vec{r}_2)^2} &= \frac{r_1^2 r_2^2 \cos^2(\phi_1 - \phi_2)}{(k_{\perp}^2 r_1^2 \cos^2\phi_1)(k_{\perp}^2 r_2^2 \cos^2\phi_2)} \\ &= \frac{(\cos\phi_1 \cos\phi_2 + \sin\phi_1 \sin\phi_2)^2}{k_{\perp}^4 \cos^2\phi_1 \cos^2\phi_2} \\ &= \frac{1}{k_{\perp}^4} (1 + 2 \tan\phi_1 \tan\phi_2 + \tan^2\phi_1 \tan^2\phi_2) . \end{aligned} \quad (3.11)$$

The first term in (3.11) explains the interaction between the endpoints of the strings with the additional factor $1/k_{\perp}^4$ in the first contribution I_{qq}^{NP} already mentioned above. The product of the second term in (3.11), $2 \tan\phi_1 \tan\phi_2$, with the dipole factors vanishes after the integration over the dipole orientations ϕ_1 and ϕ_2 . The third term in (3.11), $\tan^2\phi_1 \tan^2\phi_2$, weights the different orientations of the strings and is characteristic for the string-string interaction (3.7) in our model. Due to this factor, the string-string interaction differs significantly from the interaction between the quarks and antiquarks of the dipoles known from perturbative two-gluon exchange (3.5).

In Fig. 3, we show the perturbative integrand I^P (solid line) and the non-perturbative integrand I^{NP} (dashed line) of the total dipole-dipole cross section (3.4) as a function of transverse momentum $|\vec{k}_{\perp}|$ for various dipole sizes. The integrands have been calculated with the model parameters given in Sec. 2 that allow a good description of the experimental data of hadron and photon reactions at the c.m. energy of $\sqrt{s_0} \approx 20$ GeV with the wave functions given in Appendix A and the exact T -matrix element (2.5). Evidently, the non-perturbative integrand I^{NP} governs the low momenta and the perturbative integrand I^P the high momenta exchanged in the dipole-dipole scattering. This behavior is a direct consequence of the correlation functions: The non-perturbative correlation functions (2.22) and (2.23) favor low momenta and suppress high momenta in comparison to the perturbative correlation

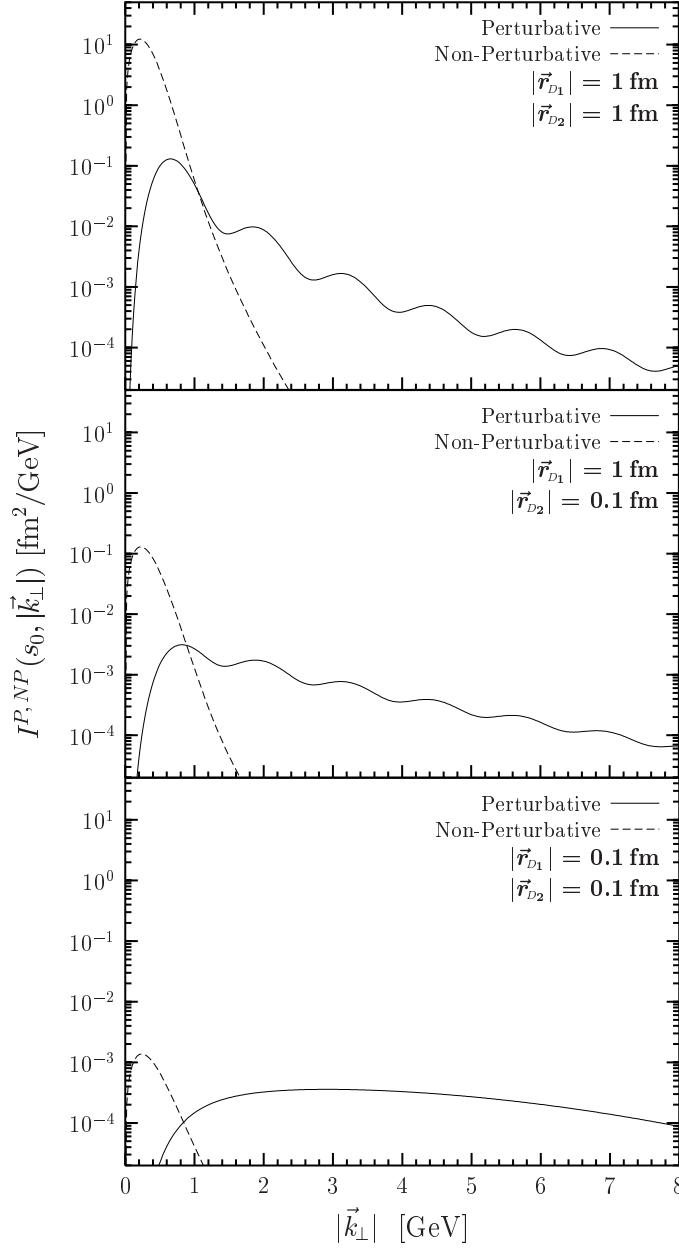


Figure 3: The perturbative integrand I^P (solid line) and the non-perturbative integrand I^{NP} (dashed line) of the total dipole-dipole cross section (3.4) as a function of transverse momentum $|\vec{k}_\perp|$ for various dipole sizes $|\vec{r}_{D1}|$ and $|\vec{r}_{D2}|$. The integrands are shown for the parameters given in Sec. 2 that allow a good description of the experimental data of hadron and photon reactions at $\sqrt{s_0} \approx 20$ GeV with the wave functions given in Appendix A and the exact T -matrix element (2.5). The oscillations of the perturbative integrand I^P originate from the Bessel function $J_0(|\vec{k}_\perp||\vec{r}_{D_i}|)$.

function (2.11). For fixed dipole sizes $|\vec{r}_{D_1}|$ and $|\vec{r}_{D_2}|$ the absolute values of the perturbative and non-perturbative integrand are controlled respectively by the parameters (m_g, M) and (G_2, a, κ) given in Sec. 2. With decreasing dipole sizes the ratio I^P/I^{NP} increases: for large dipole sizes $|\vec{r}_{D_1}| = |\vec{r}_{D_2}| = 1$ fm, the non-perturbative contribution gives the main contribution to the total dipole-dipole cross section; for small dipole sizes $|\vec{r}_{D_1}| = |\vec{r}_{D_2}| = 0.1$ fm, the perturbative contribution dominates.

As can be seen from the analytic results (3.5)–(3.10), the total dipole-dipole cross section (3.4) or the forward scattering amplitude $T(s_0, t = 0)$ does not depend on the longitudinal quark momentum fractions z_{D_i} of the dipoles. For $t = 0$ the parameter z_{D_i} disappears upon the integration over z_i since only $|\psi_{D_i}(z_i, \vec{r}_i)|^2$ (3.2) depends on z_i .

The structure presented for dipole-dipole scattering remains in reactions involving hadrons and photons: the hadronic and photonic total cross sections are obtained from the total dipole-dipole cross section (3.1) by replacing $|\psi_{D_i}(z_i, \vec{r}_i)|^2$ given in (3.2) with the hadron and photon wave functions given in Appendix A. As the total dipole-dipole cross section, the total hadronic and photonic cross sections are independent of the parameters which control the z_i -distribution in the wave functions due to the normalization of the z_i -distributions. The independence of the total hadronic cross section on the widths Δz_h can be seen immediately with the Gaussian hadron wave functions (A.1)

$$\langle \psi_h | 1 - e^{i\vec{k}_\perp \vec{r}_i} | \psi_h \rangle = 1 - e^{-\frac{1}{2} k_\perp^2 S_h^2}, \quad (3.12)$$

$$\langle \psi_h | \tan^2 \phi_i (1 - e^{i\vec{k}_\perp \vec{r}_i}) | \psi_h \rangle = -1 + e^{-\frac{1}{2} k_\perp^2 S_h^2} + \sqrt{\frac{\pi}{2}} |\vec{k}_\perp| S_h \operatorname{Erf} \left(\frac{|\vec{k}_\perp| S_h}{\sqrt{2}} \right) \quad (3.13)$$

with the error function $\operatorname{Erf}(z) = \sqrt{2/\pi} \int_0^z dt \exp(-t^2)$. These analytical results confirm the Δz_h and z_D -independence of the total dipole-proton cross section assumed in phenomenological models [29, 36]. However, the non-forward hadronic scattering amplitude $T(s_0, t \neq 0)$ depends on the parameter Δz_h as shown explicitly in Appendix B. Thus, the differential elastic cross section $d\sigma^{el}/dt(s, t)$ (B.6) and its logarithmic slope $B(s, t)$ (B.7) are Δz_h -dependent. In fact, this Δz_h -dependence is essential for the agreement with experimental data [1].

The $|\vec{k}_\perp|$ -dependence of the perturbative and non-perturbative integrand for hadron-hadron, hadron-photon, and photon-photon cross sections at high photon virtualities is similar to the one of the perturbative and non-perturbative integrand of the dipole-dipole cross section shown in Fig. 3 for $(|\vec{r}_{D_1}| = |\vec{r}_{D_2}| = 1$ fm), $(|\vec{r}_{D_1}| = 1$ fm, $|\vec{r}_{D_2}| = 0.1$ fm), and $(|\vec{r}_{D_1}| = |\vec{r}_{D_2}| = 0.1$ fm), respectively. Of course, the absolute values differ and the oscillations of the perturbative integrand caused by the Bessel functions disappear.

4 Decomposition of the QCD String into Dipoles and the Unintegrated Gluon Distribution

The *unintegrated gluon distribution* of hadrons⁹ $\mathcal{F}_h(x, k_\perp^2)$ is a basic, universal quantity convenient for the computation of many scattering observables at small x . It is the central object in the BFKL [23] and CCFM [24] evolution equations. Upon integration over the transverse gluon momentum $|\vec{k}_\perp|$ it leads to the conventional gluon distribution $xG_h(x, Q^2)$ used in the DGLAP evolution equation [25]. The unintegrated gluon distribution is crucial to describe processes in which transverse momenta are explicitly exposed such as dijet [21] or vector meson [22] production at HERA. Its explicit $|\vec{k}_\perp|$ dependence is particularly suited to study the interplay between soft and hard physics. In this section, an exact representation of the string as a collection of stringless quark-antiquark dipoles is presented that allows to extract the perturbative and non-perturbative contributions to $\mathcal{F}_h(x, k_\perp^2)$ from our total dipole-hadron cross section via $|\vec{k}_\perp|$ -factorization.

We calculate the unintegrated gluon distribution $\mathcal{F}_h(x, k_\perp^2)$ with the T -matrix element in the limit of small χ -functions (2.24). Motivated by the successful description of many data in our recent work [1] we give a strong energy dependence to the perturbative contribution χ^P and a weak one to the non-perturbative contribution χ^{NP} ,

$$\begin{aligned} (\chi^P)^2 &\rightarrow (\chi^P)^2 \left(\frac{x_0}{x}\right)^{\epsilon^P} \\ (\chi^{NP})^2 &\rightarrow (\chi^{NP})^2 \left(\frac{x_0}{x}\right)^{\epsilon^{NP}} \end{aligned} \quad (4.1)$$

where the values of the exponents $\epsilon^P = 0.73$ and $\epsilon^{NP} = 0.125$ are adopted from [1] and $x_0 = 2.4 \cdot 10^{-3}$ is adjusted to reproduce at $Q^2 = 1 \text{ GeV}^2$ the integrated gluon distribution of the proton $xG_p(x, Q^2)$ extracted from the HERA data [37]. The small- χ limit (2.24) considered here is applicable only for $x = Q^2/s \geq 10^{-4}$. At higher energies (lower Bjorken- x) the full T -matrix element (2.5) has to be used in order to satisfy unitarity constraints of the S -matrix [1, 38].

The total dipole-hadron cross section $\sigma_{Dh}(x, |\vec{r}_D|)$ is obtained from the total dipole-dipole cross section (3.1) by replacing $|\psi_{D_2}(z_2, \vec{r}_2)|^2$ with a squared hadron wave function $|\psi_h(z_2, \vec{r}_2)|^2$. Accordingly, the x -dependent total dipole-hadron cross

⁹The word hadron and the subscript h is used genuinely for hadrons and photons in this section.

section reads

$$\begin{aligned}
\sigma_{Dh}(x, |\vec{r}_D|) &= \frac{8}{9} \frac{1}{4\pi} \int dk_{\perp}^2 \tag{4.2} \\
&\times \left[(4\pi\alpha_s(k_{\perp}^2))^2 \left\{ \left[i\tilde{D}'^{(2)}(k_{\perp}^2) \right]^2 \left(1 - J_0(|\vec{k}_{\perp}||\vec{r}_D|) \right) \langle \psi_h | 1 - e^{i\vec{k}_{\perp}\vec{r}_2} | \psi_h \rangle \right\} \left(\frac{x_0}{x} \right)^{\epsilon^P} \right. \\
&+ \left(\frac{\pi^2 G_2}{24} \right)^2 \left\{ \left[\frac{\kappa}{k_{\perp}^2} i\tilde{D}^{(2)}(k_{\perp}^2) + (1 - \kappa) i\tilde{D}'^{(2)}(k_{\perp}^2) \right]^2 \left(1 - J_0(|\vec{k}_{\perp}||\vec{r}_D|) \right) \langle \psi_h | 1 - e^{i\vec{k}_{\perp}\vec{r}_2} | \psi_h \rangle \right. \\
&\left. \left. + \left[\frac{\kappa}{k_{\perp}^2} i\tilde{D}^{(2)}(k_{\perp}^2) \right]^2 \left(-1 + {}_1F_2\left(-\frac{1}{2}; \frac{1}{2}, 1; \frac{-k_{\perp}^2 r_D^2}{4}\right) \right) \langle \psi_h | \tan^2 \phi_2 (1 - e^{i\vec{k}_{\perp}\vec{r}_2}) | \psi_h \rangle \right\} \left(\frac{x_0}{x} \right)^{\epsilon^{NP}} \right]
\end{aligned}$$

with the Bessel function $J_0(|\vec{k}_{\perp}||\vec{r}_D|)$ and the generalized hypergeometric function ${}_1F_2(-1/2; 1/2, 1; -k_{\perp}^2 r_D^2/4)$ derived in the previous section.

For dipole sizes $|\vec{r}_D| \rightarrow 0$, the perturbative contribution to $\sigma_{Dh}(x, |\vec{r}_D|)$ is known to vanish quadratically with decreasing dipole size, $\sigma_{Dh}(x, |\vec{r}_D|) \propto r_D^2$. This behavior reflects the weak absorption of a small color-singlet dipole in the hadron and is known as *color transparency*. It can be seen immediately from (4.2) as

$$\left(1 - J_0(|\vec{k}_{\perp}||\vec{r}_D|) \right) \approx \frac{k_{\perp}^2 r_D^2}{4} \quad \text{for } |\vec{r}_D| \rightarrow 0 \text{ and finite } |\vec{k}_{\perp}|. \tag{4.3}$$

The non-perturbative contribution to $\sigma_{Dh}(x, |\vec{r}_D|)$ gives color transparency as well since the generalized hypergeometric function behaves as

$$\left(-1 + {}_1F_2\left(-\frac{1}{2}; \frac{1}{2}, 1; \frac{-k_{\perp}^2 r_D^2}{4}\right) \right) \approx \frac{k_{\perp}^2 r_D^2}{4} \quad \text{for } |\vec{r}_D| \rightarrow 0 \text{ and finite } |\vec{k}_{\perp}|. \tag{4.4}$$

For large dipole sizes, $|\vec{r}_D| \gtrsim 1 \text{ fm}$, the perturbative contribution to $\sigma_{Dh}(x, |\vec{r}_D|)$ describing interactions of the quark and antiquark of the dipole with the hadron saturates since

$$\left(1 - J_0(|\vec{k}_{\perp}||\vec{r}_D|) \right) \approx 1 \quad \text{for large } |\vec{k}_{\perp}||\vec{r}_D|. \tag{4.5}$$

In contrast, the non-perturbative contribution to $\sigma_{Dh}(x, |\vec{r}_D|)$ increases linearly with increasing dipole size, $\sigma_{Dh}(x, |\vec{r}_D|) \propto |\vec{r}_D|$. This linear increase is generated by the interaction of the string of the dipole with the hadron: The string elongates linearly with the dipole size $|\vec{r}_D|$ and, thus, has a linearly increasing geometric cross section with the hadron. Indeed, this feature of the string can be seen analytically since

$$\left(-1 + {}_1F_2\left(-\frac{1}{2}; \frac{1}{2}, 1; \frac{-k_{\perp}^2 r_D^2}{4}\right) \right) \propto |\vec{k}_{\perp}||\vec{r}_D| \quad \text{for large } |\vec{k}_{\perp}||\vec{r}_D|. \tag{4.6}$$

When considered in Euclidean space-time, the same string gives also the linear confining potential between a static quark and antiquark at large $q\bar{q}$ separations [10, 11]. Obviously, the behavior of the total dipole-hadron cross section is related to the confining potential. Furthermore, as we are working in the quenched approximation, there is no string breaking through dynamical quark-antiquark production at large dipole sizes. String breaking is expected to stop the linear increase of the total dipole-hadron cross section at dipole sizes of $|\vec{r}_D| \gtrsim 1$ fm analogous to the saturation of the static $q\bar{q}$ potential seen for large $q\bar{q}$ separations on the lattice in full QCD [39, 40].

In Fig. 4, we show the perturbative (solid line) and non-perturbative (dashed line) contributions to the total dipole-proton cross section $\sigma_{Dp}(x, |\vec{r}_D|)$ as a function of the dipole size $|\vec{r}_D|$ at $x = x_0 = 2.4 \cdot 10^{-3}$, where the perturbative contribution is multiplied by a factor of 10. The dipole-proton cross section is computed with

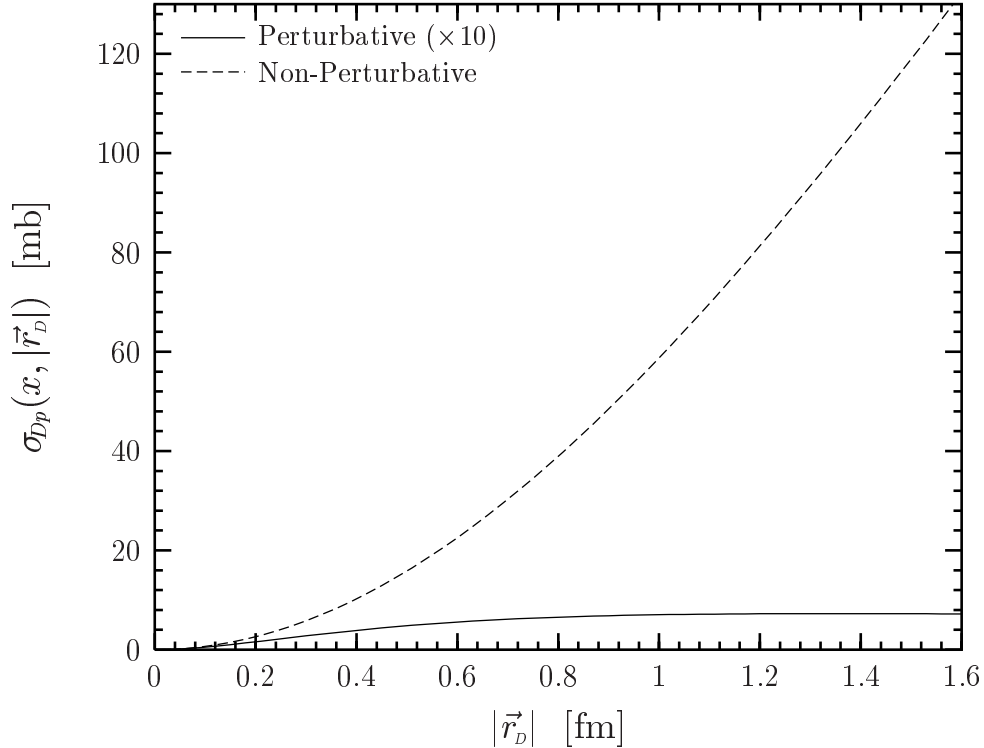


Figure 4: Perturbative (solid line) and non-perturbative (dashed line) contributions to the total dipole-proton cross section $\sigma_{Dp}(x, |\vec{r}_D|)$ as a function of the dipole size $|\vec{r}_D|$ at $x = x_0 = 2.4 \cdot 10^{-3}$. with the perturbative contribution multiplied by a factor of 10. The perturbative contribution shows color transparency at small $|\vec{r}_D|$ and saturates at large $|\vec{r}_D|$. The non-perturbative contribution shows also color transparency at small $|\vec{r}_D|$ but increases linearly with increasing $|\vec{r}_D|$.

the simple Gaussian proton wave function (A.1) and illustrates the general features discussed above: The perturbative contribution shows color transparency at small $|\vec{r}_D|$ and saturates at large $|\vec{r}_D|$. The non-perturbative contribution shows also color transparency at small $|\vec{r}_D|$ but increases linearly with increasing $|\vec{r}_D|$.

Our result (4.2) shows that the $|\vec{k}_\perp|$ -dependence of the hadron constituents factorizes from the rest of the process in both the perturbative and the non-perturbative contribution to the total dipole-hadron cross section. This factorization – known in perturbative QCD as $|\vec{k}_\perp|$ -factorization [41] – allows to define the unintegrated gluon distribution $\mathcal{F}_h(x, k_\perp^2)$ as follows [42–44]

$$\sigma_{Dh}(x, |\vec{r}_D|) = \frac{4\pi^2 r_D^2}{3} \int dk_\perp^2 \frac{\left(1 - J_0(|\vec{k}_\perp| |\vec{r}_D|)\right)}{(|\vec{k}_\perp| |\vec{r}_D|)^2} \alpha_s(k_\perp^2) \mathcal{F}_h(x, k_\perp^2) . \quad (4.7)$$

For small dipole sizes $|\vec{r}_D|$, this equation together with (4.3) and the integrated gluon distribution

$$xG_h(x, Q^2) = \int_0^{Q^2} dk_\perp^2 \mathcal{F}_h(x, k_\perp^2) \quad (4.8)$$

leads to the widely used perturbative QCD relation [45]

$$\sigma_{Dh}(x, |\vec{r}_D|) = \frac{\pi^2 r_D^2}{3} [\alpha_s(Q^2) xG_h(x, Q^2)]_{Q^2=c/r_D^2} , \quad (4.9)$$

where $c \approx 10$ is estimated from the properties of the Bessel function $J_0(|\vec{k}_\perp| |\vec{r}_D|)$ [46].

To extract the unintegrated gluon distribution $\mathcal{F}_h(x, k_\perp^2)$, we compare (4.7) with (4.2) using the following mathematical identity

$$\left(-1 + {}_1F_2\left(-\frac{1}{2}; \frac{1}{2}, 1; \frac{-k_\perp^2 r_D^2}{4}\right)\right) = \int_0^1 d\xi \frac{1}{\xi^2} \left(1 - J_0(|\vec{k}_\perp| |\vec{r}_D| \xi)\right) . \quad (4.10)$$

As discussed in the previous section, the lhs of (4.10) results from the string averaged over all orientations (3.10). Thus, the string confining the quark-antiquark dipole of length $|\vec{r}_D|$ can be represented as an integral over stringless dipoles of sizes $\xi|\vec{r}_D|$ with $0 \leq \xi \leq 1$ and a dipole number density of $n(\xi) = 1/\xi^2$. As visualized in Fig. 5, the string-hadron scattering process reduces to an incoherent superposition of stringless dipole-hadron scattering processes with dipole sizes $0 \leq \xi|\vec{r}_D| \leq |\vec{r}_D|$ and dipole number density $n(\xi) = 1/\xi^2$. The decomposition of the string into many smaller stringless dipoles via (4.10) behaves similar to the wave function of a $q\bar{q}$ onium state in the large N_c limit [47, 48]: The numerous gluons emitted inside the onium state can be considered as many $q\bar{q}$ dipoles in the large N_c limit.

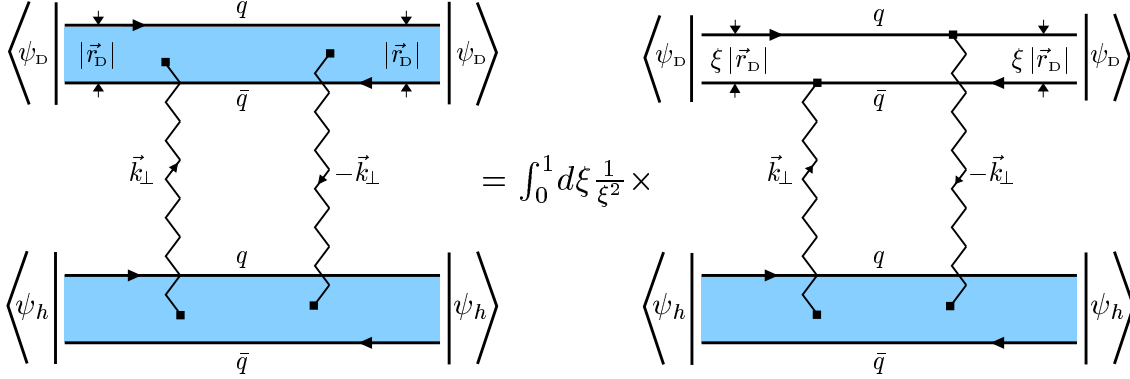


Figure 5: The string of length $|\vec{r}_D|$ is made up of stringless dipoles of size $\xi|\vec{r}_D|$ with $0 \leq \xi \leq 1$ and dipole number density $n(\xi) = 1/\xi^2$. The string-hadron scattering process reduces to an incoherent superposition of stringless dipole-hadron scattering processes.

Inserting (4.10) into (4.2) and rescaling the momentum variable $|\vec{k}'_\perp| = \xi|\vec{k}_\perp|$, the string-hadron (sh) contribution to the total dipole-hadron cross section (4.2) becomes

$$\begin{aligned} \sigma_{Dh}^{sh}(x, |\vec{r}_D|) &= \frac{8}{9} \frac{1}{4\pi} \int dk_\perp'^2 \left(1 - J_0(|\vec{k}'_\perp| |\vec{r}_D|)\right) \\ &\times \left(\frac{\pi^2 G_2}{24}\right)^2 \left\{ \frac{\kappa^2}{k_\perp'^4} \int_0^1 d\xi \left[i\tilde{D}^{(2)}\left(\frac{k_\perp'^2}{\xi^2}\right) \right]^2 \langle \psi_h | \tan^2 \phi_2 (1 - e^{i(\vec{k}'_\perp/\xi)\vec{r}_2}) | \psi_h \rangle \right\} \left(\frac{x_0}{x}\right)^{\epsilon^{NP}}. \end{aligned} \quad (4.11)$$

The dipole factor $(1 - J_0(|\vec{k}'_\perp| |\vec{r}_D|))$ indicates that the string-hadron interaction has been rewritten into a stringless dipole-hadron interaction. The string confining the dipole has been shifted into the hadron. Comparing (4.7) with our new expression for the total dipole-hadron cross section,

$$\begin{aligned} \sigma_{Dh}(x, |\vec{r}_D|) &= \frac{8}{9} \frac{1}{4\pi} \int dk_\perp^2 \left(1 - J_0(|\vec{k}_\perp| |\vec{r}_D|)\right) \\ &\times \left[(4\pi\alpha_s(k_\perp^2))^2 \left\{ \left[i\tilde{D}'_P(2)(k_\perp^2) \right]^2 \langle \psi_h | 1 - e^{i\vec{k}_\perp \vec{r}_2} | \psi_h \rangle \right\} \left(\frac{x_0}{x}\right)^{\epsilon^P} \right. \\ &+ \left(\frac{\pi^2 G_2}{24}\right)^2 \left\{ \left[(1 - \kappa) \left[i\tilde{D}'_1(2)(k_\perp^2) \right] + \frac{\kappa}{k_\perp^2} \left[i\tilde{D}^{(2)}(k_\perp^2) \right] \right]^2 \langle \psi_h | 1 - e^{i\vec{k}_\perp \vec{r}_2} | \psi_h \rangle \right. \\ &\left. \left. + \frac{\kappa^2}{k_\perp^4} \int_0^1 d\xi \left[i\tilde{D}^{(2)}\left(\frac{k_\perp^2}{\xi^2}\right) \right]^2 \langle \psi_h | \tan^2 \phi_2 (1 - e^{i(\vec{k}_\perp/\xi)\vec{r}_2}) | \psi_h \rangle \right\} \left(\frac{x_0}{x}\right)^{\epsilon^{NP}} \right], \end{aligned} \quad (4.12)$$

one obtains the unintegrated gluon distribution

$$\begin{aligned}
\mathcal{F}_h(x, k_\perp^2) &= \frac{k_\perp^2}{6\pi^3\alpha_s(k_\perp^2)} \\
&\times \left[(4\pi\alpha_s(k_\perp^2))^2 \left\{ \left[i\tilde{D}'_P(2)(k_\perp^2) \right]^2 \langle \psi_h | 1 - e^{i\vec{k}_\perp \vec{r}_2} | \psi_h \rangle \right\} \left(\frac{x_0}{x} \right)^{\epsilon_P} \right. \\
&+ \left(\frac{\pi^2 G_2}{24} \right)^2 \left\{ \left[(1 - \kappa) \left[i\tilde{D}'_1(2)(k_\perp^2) \right] + \frac{\kappa}{k_\perp^2} \left[i\tilde{D}(2)(k_\perp^2) \right] \right]^2 \langle \psi_h | 1 - e^{i\vec{k}_\perp \vec{r}_2} | \psi_h \rangle \right. \\
&\left. \left. + \frac{\kappa^2}{k_\perp^4} \int_0^1 d\xi \left[i\tilde{D}(2)\left(\frac{k_\perp^2}{\xi^2}\right) \right]^2 \langle \psi_h | \tan^2\phi_2(1 - e^{i(\vec{k}_\perp/\xi)\vec{r}_2}) | \psi_h \rangle \right\} \left(\frac{x_0}{x} \right)^{\epsilon_{NP}} \right]. \quad (4.13)
\end{aligned}$$

This result shows explicitly the microscopic structure of the perturbative and non-perturbative contribution to $\mathcal{F}_h(x, k_\perp^2)$. It is valid for any hadron wave function. To get numerical values for the unintegrated gluon distribution $\mathcal{F}_h(x, k_\perp^2)$, the hadron wave functions must be specified.

5 Numerical Results for the Unintegrated Gluon Distribution in Hadrons and Photons

In this section, we present the unintegrated gluon distribution (4.13) for protons, pions, kaons, and photons computed with the Gaussian hadron wave function (A.1) and the perturbatively derived photon wave functions (A.2) and (A.3). To account for non-perturbative effects at low photon virtuality Q^2 in the photon wave functions, quark masses $m_f(Q^2)$ are used that interpolate between the current quarks at large Q^2 and the constituent quarks at small Q^2 [15] as discussed in Appendix A.

The unintegrated gluon distribution of the proton $\mathcal{F}_p(x, k_\perp^2)$ is shown as a function of transverse momentum $|\vec{k}_\perp|$ at $x = 10^{-1}$, 10^{-2} , 10^{-3} , and 10^{-4} in Fig. 6. Figure 7 illustrates the interplay of the perturbative (solid line) and non-perturbative (dashed line) contributions to $|\vec{k}_\perp| \mathcal{F}_p(x, k_\perp^2)$ as a function of transverse momentum $|\vec{k}_\perp|$ for the same values of x . At small momenta $|\vec{k}_\perp|$, the unintegrated gluon distribution is dominated by the non-perturbative contribution and behaves as $1/|\vec{k}_\perp|$. This behavior reflects the linear increase of the total dipole-proton cross section at large dipole sizes. In contrast, the saturation model of Golec-Biernat and Wüsthoff [44] shows the behavior $\mathcal{F}_p^{GBW}(x, k_\perp^2) \propto k_\perp^2$ for small momenta. With increasing $|\vec{k}_\perp|$, the non-perturbative contribution to $\mathcal{F}_p(x, k_\perp^2)$ decreases rapidly which results from the strong suppression of large momenta by the non-perturbative correlation functions

$i\tilde{D}'^{(2)}(k_{\perp}^2)$ and $i\tilde{D}^{(2)}(k_{\perp}^2)$ given in (2.22) and (2.23). For $|\vec{k}_{\perp}| \gtrsim 1$ GeV, the perturbative contribution dominates the unintegrated gluon distribution. It drops as $1/k_{\perp}^2$ in accordance with the perturbative correlation function $i\tilde{D}'^{(2)}(k_{\perp}^2)$ given in (2.21). This perturbative QCD result is not reproduced by the phenomenological model of Golec-Biernat and Wüsthoff [44] which predicts a Gaussian decrease of $\mathcal{F}_p(x, k_{\perp}^2)$ with increasing $|\vec{k}_{\perp}|$.

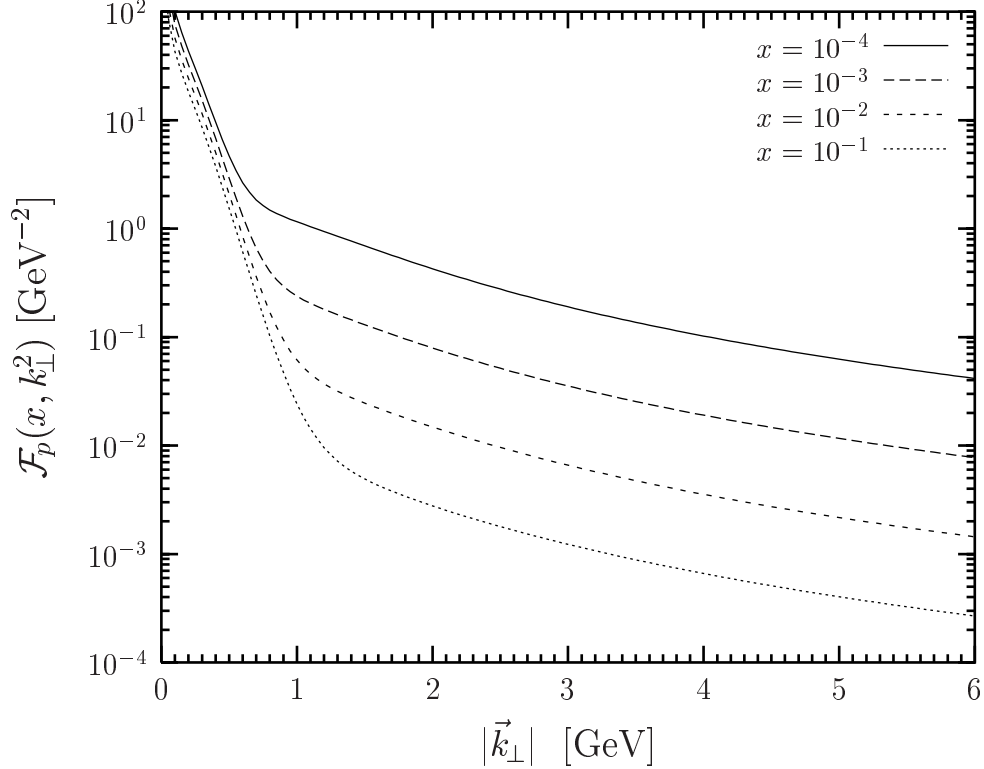


Figure 6: The unintegrated gluon distribution of the proton $\mathcal{F}_p(x, k_{\perp}^2)$ as a function of transverse momentum $|\vec{k}_{\perp}|$ at Bjorken- x values of 10^{-1} , 10^{-2} , 10^{-3} and 10^{-4} .

The x -dependence of $\mathcal{F}_p(x, k_{\perp}^2)$ can be seen in Figs. 6 and 7: With decreasing x , the perturbative contribution increases much stronger than the non-perturbative contribution which results from the energy exponents $\epsilon^P \gg \epsilon^{NP}$ in (4.1) necessary to describe the data within our model [1]. Moreover, the perturbative contribution extends into the small- $|\vec{k}_{\perp}|$ region as x decreases. Indeed, the soft-hard transition point moves towards smaller momenta with decreasing x as shown in Fig. 7. Such a hard-to-soft diffusion is observed also in [49] where the unintegrated gluon distribution has been parametrized to reproduce the experimental data for the proton structure function $F_2(x, Q^2)$ at small x . The opposite behavior is obtained in the

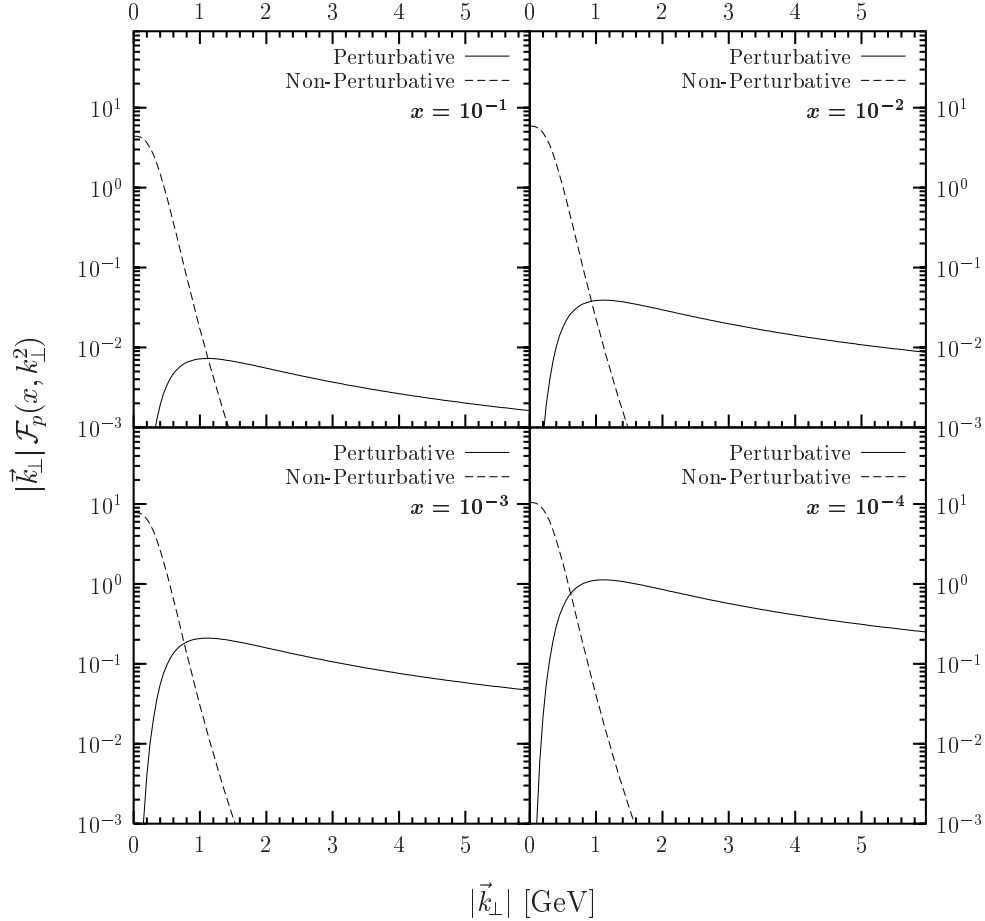


Figure 7: The unintegrated gluon distribution of the proton $\mathcal{F}_p(x, k_\perp^2)$ times the transverse momentum $|\vec{k}_\perp|$ as a function of $|\vec{k}_\perp|$ at Bjorken- x values of 10^{-1} , 10^{-2} , 10^{-3} and 10^{-4} .

approach of the color glass condensate [50]: With decreasing x , gluons are produced predominantly in the high- $|\vec{k}_\perp|$ region of lower density and weaker repulsive interactions.

In Fig. 8, the unintegrated gluon distribution of the proton, pion, and kaon $\mathcal{F}_h(x, k_\perp^2)$ times the transverse momentum $|\vec{k}_\perp|$ is shown as a function of $|\vec{k}_\perp|$ at $x = 10^{-3}$. The hadrons are characterized by different values for Δz_h and S_h in the hadron wave function (A.1). However, $\mathcal{F}_h(x, k_\perp^2)$ depends only on S_h . Due to the normalization of the hadron wave functions, Δz_h disappears upon the integration over z_i as can be seen directly from (3.12) and (3.13). At small momenta, $\mathcal{F}_h(x, k_\perp^2) \propto S_h^2$ is found from (3.12), (3.13), and (4.13). It becomes visible in Fig. 8 for the chosen hadron extensions: $S_p = 0.86$ fm, $S_\pi = 0.607$ fm, and $S_K = 0.55$ fm. At

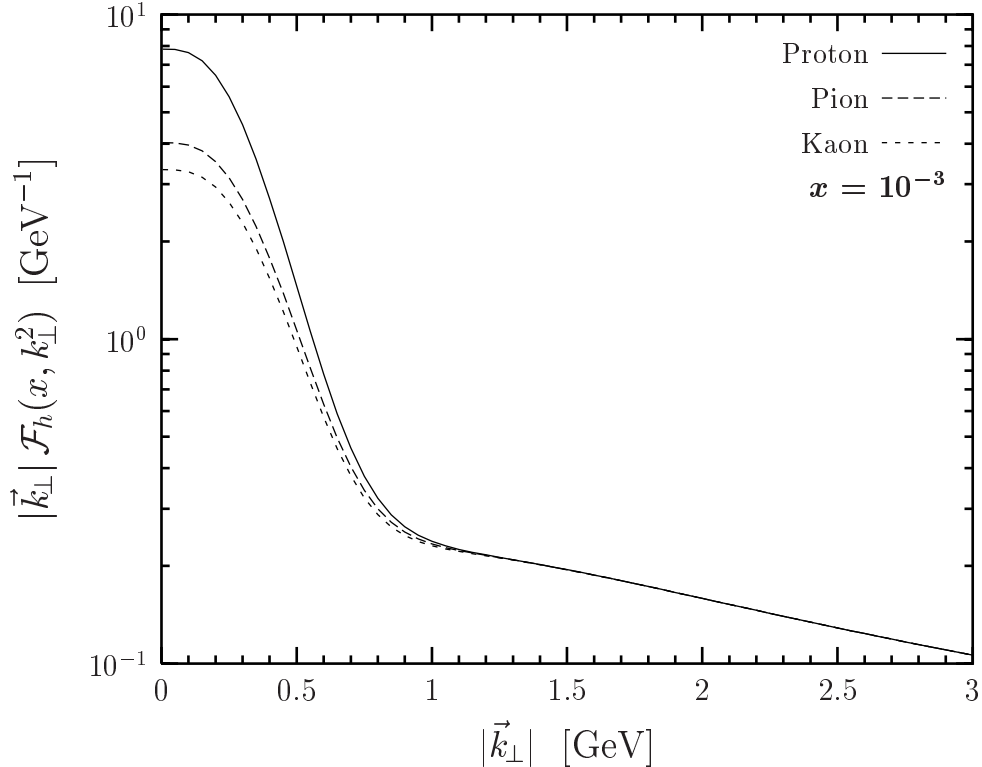


Figure 8: The unintegrated gluon distribution of the proton, pion, and kaon $\mathcal{F}_h(x, k_\perp^2)$ times the transverse momentum $|\vec{k}_\perp|$ as a function of $|\vec{k}_\perp|$ at Bjorken-variable $x = 10^{-3}$.

large momenta where the perturbative contribution dominates, the dependence on S_h vanishes as can be seen from (3.12) and the unintegrated gluon distributions of protons, pions, and kaons become identical. Of course, this behavior results from the wave function normalization being identical for protons, pions, and kaons with two valence constituents which are the quark and antiquark in the pion and kaon and the quark and diquark in the proton. At large $|\vec{k}_\perp|$, i.e., high resolution, the realistic description of protons as three-quark systems becomes necessary. In fact, the three-quark description of protons leads to a different perturbative contribution in (4.13): the quark counting factors of 2 (appropriate for mesons) in the square brackets in (3.5) are substituted by factors of 3 (appropriate for baryons) [19, 20]. At other values of x , the unintegrated gluon distributions of protons, pions and kaons show the same features.

Photons are particularly interesting because the transverse size of the quark-antiquark dipole into which a photon fluctuates is controlled by the photon virtual-

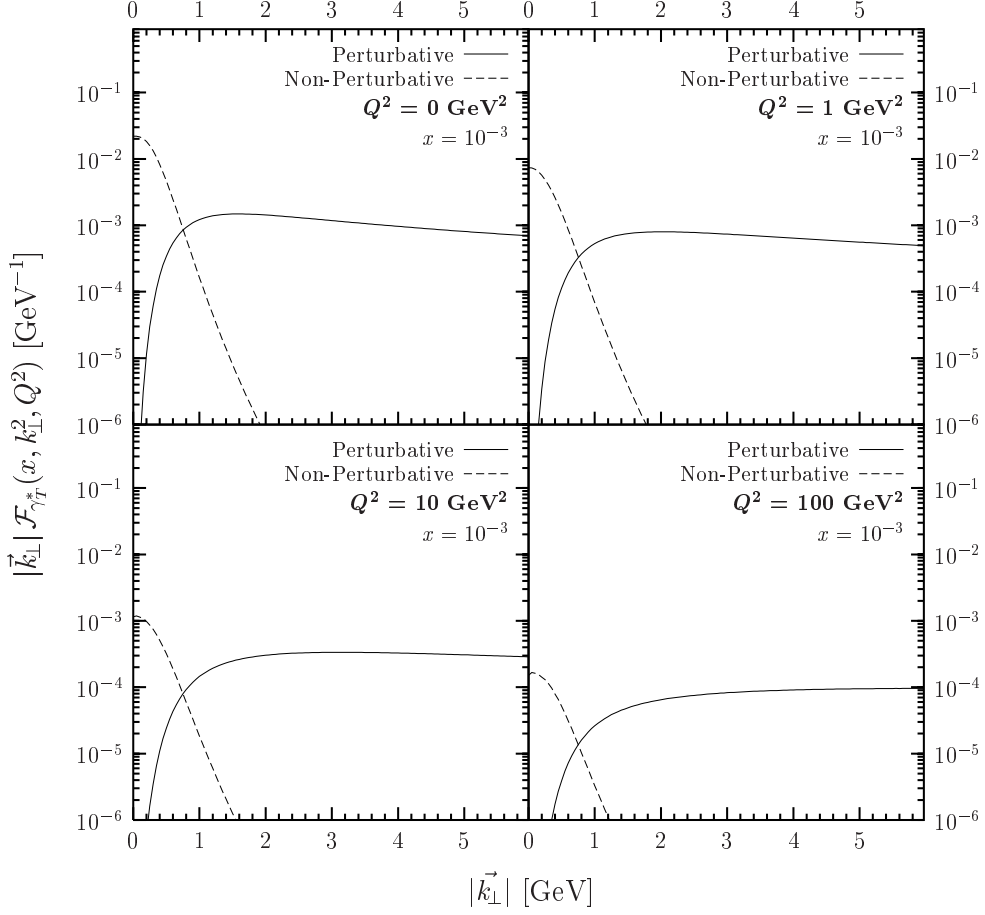


Figure 9: The unintegrated gluon distribution of the transverse polarized photon $\mathcal{F}_{\gamma_T^*}(x, k_\perp^2, Q^2)$ times the transverse momentum $|\vec{k}_\perp|$ as a function of $|\vec{k}_\perp|$ at photon virtualities of $Q^2 = 0, 1, 10, \text{ and } 100 \text{ GeV}^2$ and Bjorken-variable $x = 10^{-3}$.

ity Q^2 (cf. Appendix A)

$$|\vec{r}_{\gamma_{T,L}^*}| \approx \frac{2}{Q^2 + 4m_u^2(Q^2)}, \quad (5.1)$$

where $m_u(Q^2)$ is the running u -quark mass given in Appendix A. In Figs. 9 and 10, the unintegrated gluon distribution of transverse (T) and longitudinal (L) photons $\mathcal{F}_{\gamma_{T,L}^*}(x, k_\perp^2, Q^2)$ times the transverse momentum $|\vec{k}_\perp|$ is shown as a function of $|\vec{k}_\perp|$ for various photon virtualities Q^2 at $x = 10^{-3}$. With increasing Q^2 , i.e., decreasing “photon size” $|\vec{r}_{\gamma_{T,L}^*}|$, the ratio of the perturbative to the non-perturbative contribution to $\mathcal{F}_{\gamma_{T,L}^*}(x, k_\perp^2, Q^2)$ increases. This behavior has already been discussed in Sec. 3 on the level of dipole-dipole scattering, where decreasing dipole sizes increase

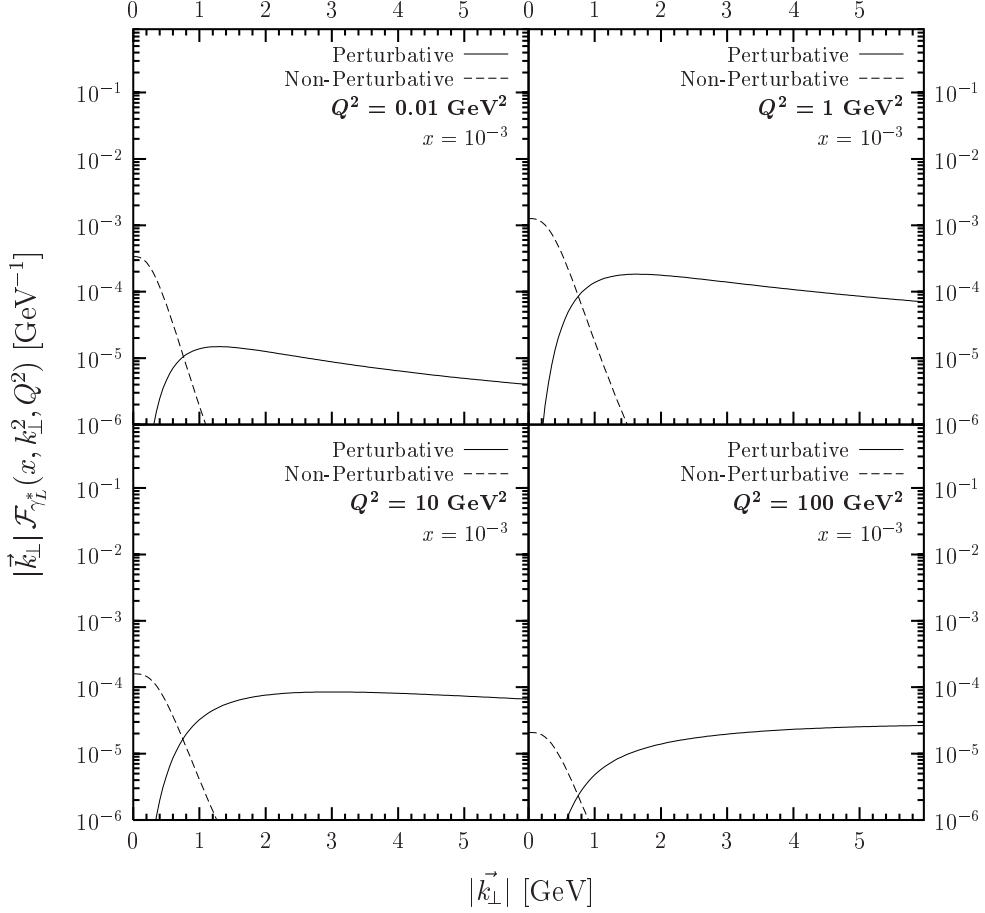


Figure 10: The unintegrated gluon distribution of the longitudinally polarized photon $\mathcal{F}_{\gamma_L^*}(x, k_\perp^2, Q^2)$ times the transverse momentum $|\vec{k}_\perp|$ as a function of $|\vec{k}_\perp|$ at photon virtualities of $Q^2 = 0.01, 1, 10,$ and 100 GeV^2 and Bjorken-variable $x = 10^{-3}$.

the ratio of the perturbative to non-perturbative contribution, see Fig. 2. Due to the different Q^2 -dependence in the transverse and longitudinally polarized photon wave functions, $\mathcal{F}_{\gamma_T^*}(x, k_\perp^2, Q^2)$ decreases continuously with increasing Q^2 while $\mathcal{F}_{\gamma_L^*}(x, k_\perp^2, Q^2)$ increases for $Q^2 \lesssim 1 \text{ GeV}^2$ and decreases for $Q^2 \gtrsim 1 \text{ GeV}^2$.

In Fig. 11, the unintegrated gluon distributions of hadrons and photons discussed above are compared. The unintegrated gluon distribution of real ($Q^2 = 0$) photons ($|\vec{r}_{\gamma_T}| \approx S_h$) is suppressed by a factor of order α in comparison to the one of the hadrons otherwise its shape is very similar. The suppression factor comes from the photon-dipole transition described by the photon wave functions given in Appendix A. The ratio of the perturbative to the non-perturbative contribution

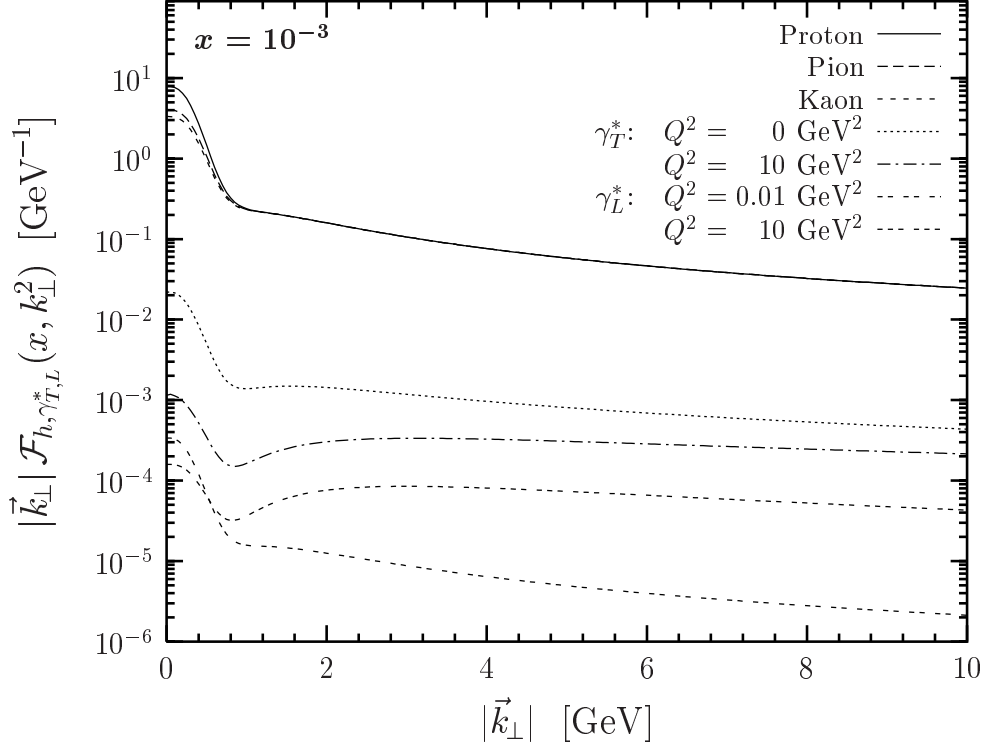


Figure 11: The unintegrated gluon distribution of the proton, pion, kaon, and transverse and longitudinally polarized photon $\mathcal{F}_{h,\gamma_{T,L}^*}(x, k_{\perp}^2)$ times the transverse momentum $|\vec{k}_{\perp}|$ as a function of $|\vec{k}_{\perp}|$ at Bjorken-variable $x = 10^{-3}$. Results for transverse polarized photons are shown for photon virtualities of $Q^2 = 0$ and 10 GeV^2 and results for longitudinally polarized photons for photon virtualities of $Q^2 = 0.01$ and 10 GeV^2 .

of unintegrated gluon distributions increases as one goes from hadrons to photons with high virtuality Q^2 . Since the wave functions of protons, pions, and kaons are normalized to the same value, the unintegrated gluon distributions of these hadrons are, as mentioned above, identical at large $|\vec{k}_{\perp}|$ and do not depend on the hadron size. In contrast, the Q^2 -dependence of the photon wave functions leads to Q^2 -dependent, i.e., “photon size”-dependent, unintegrated gluon distributions at large $|\vec{k}_{\perp}|$. With increasing $|\vec{k}_{\perp}|$, the unintegrated gluon distributions of hadrons and photons become parallel in line with the vanishing dependence on the specific form of the wave function.

In Fig. 12, the integrated gluon distribution of the proton $xG_p(x, Q^2)$ is shown as a function of Bjorken- x at photon virtualities of $Q^2 = 1, 5,$ and 20 GeV^2 . Recall that the parameter $x_0 = 2.4 \cdot 10^{-3}$ has been adjusted in the previous section such that the experimental data of $xG_p(x, Q^2)$ at $Q^2 = 1 \text{ GeV}^2$ [37] are reproduced. For

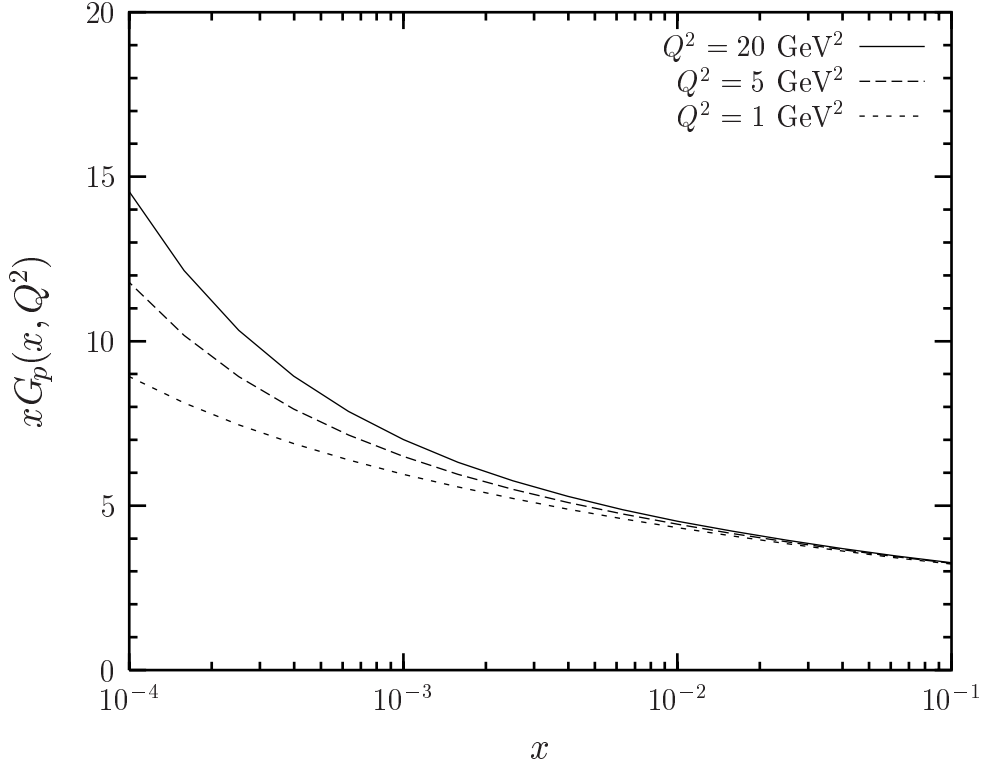


Figure 12: The gluon distribution of the proton $xG_p(x, Q^2)$ as a function of Bjorken- x at photon virtualities of $Q^2 = 1, 5,$ and 20 GeV^2 .

$x \gtrsim 10^{-3}$, $xG_p(x, Q^2)$ is mainly determined by non-perturbative physics as can be seen from Figs. 6 and 7. Perturbative physics becomes relevant for $x \lesssim 10^{-3}$ and generates the steep increase of $xG_p(x, Q^2)$ with decreasing x at fixed Q^2 . Also the rise of $xG_p(x, Q^2)$ with increasing Q^2 at fixed x results from the perturbative contribution. For $x \ll 10^{-4}$, we have shown explicitly in our recent work [1, 38] that multiple gluonic exchanges contained in the full T -matrix element (2.5) slow down the powerlike increase of $xG_p(x, Q^2)$ with decreasing x in accordance with S -matrix unitarity constraints.

6 Comparison with Other Work

In this section, we compare the unintegrated gluon distribution of the proton extracted from our loop-loop correlation model (LLCM) with those obtained from the saturation model of Golec-Biernat and Wüsthoff (GBW) [44], the derivative of the Glück, Reya, and Vogt (GRV) parametrization of $xG_p(x, Q^2)$ [51], and the approach of Ivanov and Nikolaev (IN) [49].

In the approach of Golec-Biernat and Wüsthoff [44], the unintegrated gluon distribution of the proton is extracted from the total dipole-proton cross section by inverting (4.7),

$$\mathcal{F}_p(x, k_\perp^2) = \frac{3\sigma_0}{4\pi^2\alpha_s} R_0^2(x) k_\perp^2 \exp(-R_0^2(x) k_\perp^2) \quad \text{with} \quad R_0^2(x) = \frac{1}{Q_0^2} \left(\frac{x}{x_0}\right)^\lambda \quad (6.1)$$

where the parameter $\sigma_0 = 29.12$ mb, $\alpha_s = 0.2$, $Q_0 = 1$ GeV, $\lambda = 0.277$, and $x_0 = 0.41 \cdot 10^{-4}$ are obtained from a fit to the proton structure function $F_2(x, Q^2)$ including charm quarks in the photon wave function. Note, however that the GBW approach uses the dipole-proton cross section of the GBW model on the lhs of (4.7) which implies multiple gluon exchanges while the rhs of (4.7) describes only two-gluon exchange as discussed in Sec. 3. Moreover, as demonstrated below, the large k_\perp^2 -behavior of the unintegrated gluon distribution (6.1) deviates significantly from the DGLAP results. This mismatch motivated the recent modifications of the saturation model [52].

The unintegrated gluon distribution of the proton is also computed from the integrated gluon distribution $xG_p(x, Q^2)$ by inverting (4.8)

$$\mathcal{F}_p(x, k_\perp^2) = \left. \frac{dxG_p(x, Q^2)}{dQ^2} \right|_{Q^2=k_\perp^2}. \quad (6.2)$$

Here, we use for the integrated gluon distribution $xG_p(x, Q^2)$ the leading order (LO) parametrization of Glück, Reya, and Vogt (GRV) [51], which covers the kinematic region $10^{-9} < x < 1$ and $0.8 \text{ GeV}^2 < Q^2 < 10^6 \text{ GeV}^2$.

Ivanov and Nikolaev [49] have constructed a two-component (soft + hard) ansatz for the unintegrated gluon distribution of the proton

$$\mathcal{F}_p(x, k_\perp^2) = \mathcal{F}_{\text{soft}}(x, k_\perp^2) \frac{k_s^2}{k_\perp^2 + k_s^2} + \mathcal{F}_{\text{hard}}(x, k_\perp^2) \frac{k_\perp^2}{k_\perp^2 + k_h^2} \quad (6.3)$$

with the soft and hard component

$$\mathcal{F}_{\text{soft}}(k_{\perp}^2) = a_{\text{soft}} C_F N_c \frac{\alpha_s(k_{\perp}^2)}{\pi} \frac{k_{\perp}^2}{(k_{\perp}^2 + \mu_{\text{soft}}^2)^2} \left[1 - \left(1 + \frac{3 k_{\perp}^2}{\Lambda^2} \right)^{-2} \right] \quad (6.4)$$

$$\mathcal{F}_{\text{hard}}(x, k_{\perp}^2) = \mathcal{F}_{\text{pt}}^{(B)}(k_{\perp}^2) \frac{\mathcal{F}_{\text{pt}}(x, Q_c^2)}{\mathcal{F}_{\text{pt}}^{(B)}(Q_c^2)} \Theta(Q_c^2 - k_{\perp}^2) + \mathcal{F}_{\text{pt}}(x, k_{\perp}^2) \Theta(k_{\perp}^2 - Q_c^2) \quad (6.5)$$

where $\mathcal{F}_{\text{pt}}^{(B)}(k_{\perp}^2)$ has the same form as (6.4) with the parameters a_{pt} and μ_{pt} instead of a_{soft} and μ_{soft} and $\mathcal{F}_{\text{pt}}(x, k_{\perp}^2)$ is the derivative of the integrated gluon distribution (6.2). In the IN approach, the running coupling is given by $\alpha_s(k_{\perp}^2) = \min\{0.82, (4\pi)/(\beta_0 \log[k_{\perp}^2/\Lambda_{QCD}^2])\}$. With the GRV-parametrization [51] for the integrated gluon distribution, the structure function of the proton $F_2(x, Q^2)$ has been described successfully using the following parameters: $k_s^2 = 3 \text{ GeV}^2$, $k_h^2 = (1 + 0.0018 \log(1/x^4))^{0.5}$, $a_{\text{soft}} = 2$, $a_{\text{pt}} = 1$, $\mu_{\text{soft}} = 0.1 \text{ GeV}$, $\mu_{\text{pt}} = 0.75 \text{ GeV}$, $Q_c^2 = 0.895 \text{ GeV}^2$, $\beta_0 = 9$, and $\Lambda_{QCD} = 0.2 \text{ GeV}$.

In Fig. 13, we show the LLCM, GBW, GRV, and IN results for the unintegrated gluon distribution of the proton $\mathcal{F}_p(x, k_{\perp}^2)$ as a function of transverse momentum squared k_{\perp}^2 for $x = 10^{-1}$, 10^{-2} , 10^{-3} , and 10^{-4} . At small transverse momenta, $k_{\perp}^2 \lesssim 0.1 \text{ GeV}^2$, our model gives the largest values for $\mathcal{F}_p(x, k_{\perp}^2)$. As mentioned in the previous section, our LLCM unintegrated gluon distribution increases as $1/\sqrt{k_{\perp}^2}$ with decreasing k_{\perp}^2 as a consequence of the linear increase of the total dipole-proton cross section at large dipole sizes. In contrast, for $k_{\perp}^2 \rightarrow 0$, the unintegrated gluon distribution of GBW decreases as k_{\perp}^2 and the one of IN as k_{\perp}^4 . In the perturbative region, $k_{\perp}^2 \gtrsim 1 \text{ GeV}^2$, the unintegrated gluon distribution of the LLCM becomes smaller than the one of GRV and IN but is still larger than the one of GBW. Moreover, the LLCM, GRV, and IN unintegrated gluon distributions become parallel for $x \lesssim 10^{-2}$ and drop as $1/k_{\perp}^2$ for large k_{\perp}^2 . This perturbative QCD behavior is not reproduced by the GBW unintegrated gluon distribution which decreases exponentially with increasing k_{\perp}^2 .

The x -dependence of the LLCM, GBW, GRV, and IN unintegrated gluon distributions $\mathcal{F}_p(x, k_{\perp}^2)$ is shown for transverse momenta squared $k_{\perp}^2 = 0.1, 0.5, 10$, and 50 GeV^2 in Fig. 14. In the non-perturbative region, $k_{\perp}^2 = 0.1 \text{ GeV}^2$ and $k_{\perp}^2 = 0.5 \text{ GeV}^2$, the LLCM, GBW, and IN unintegrated gluon distributions show a weak x -dependence. In the perturbative region, $k_{\perp}^2 = 10 \text{ GeV}^2$ and $k_{\perp}^2 = 50 \text{ GeV}^2$, the x -dependence of the unintegrated gluon distributions becomes stronger. The LLCM, GRV, and IN unintegrated gluon distributions show nearly the same rise with decreasing x . In contrast, the GBW unintegrated gluon distribution increases much faster as x decreases.

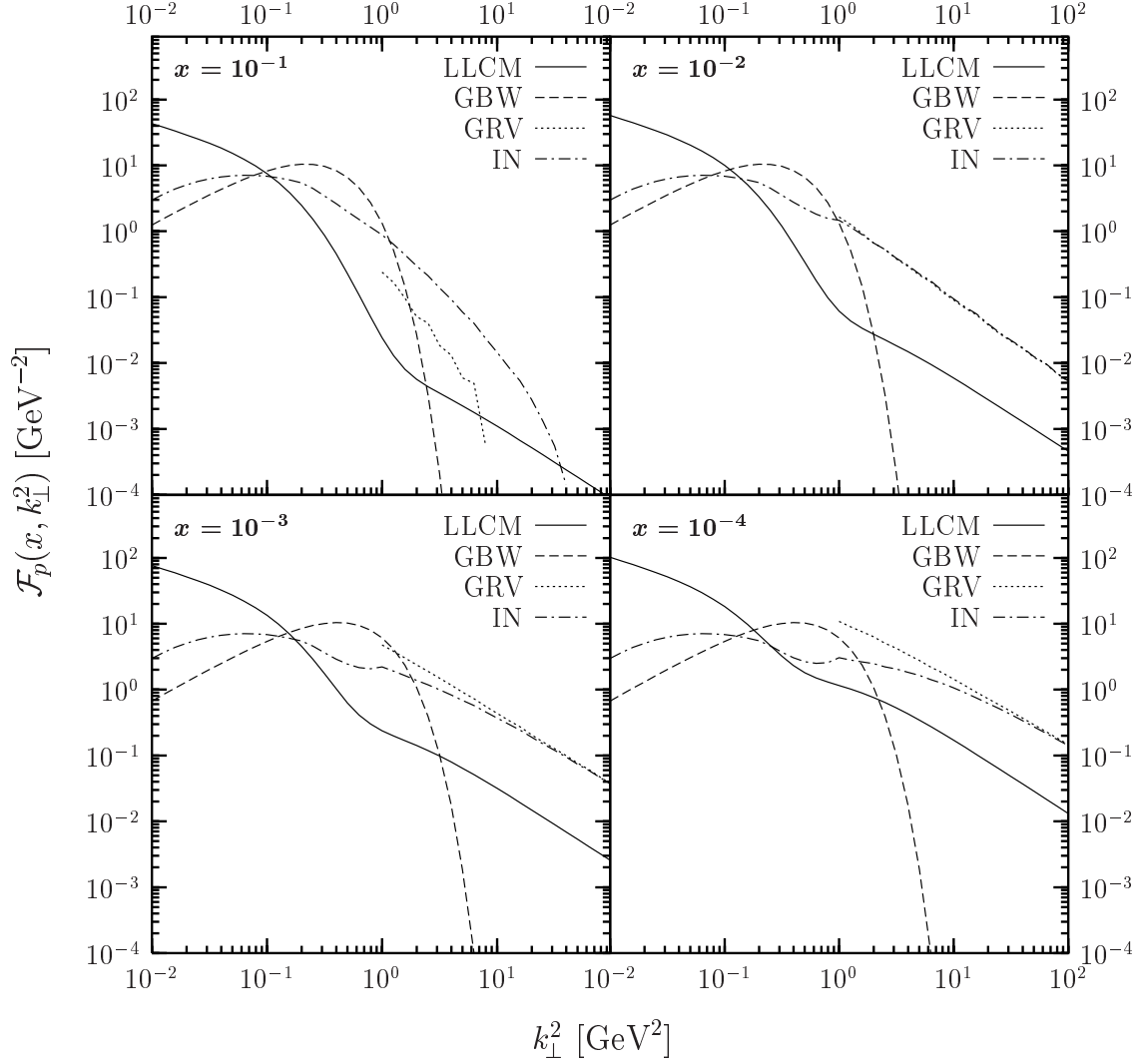


Figure 13: The unintegrated gluon distribution of the proton $\mathcal{F}_p(x, k_\perp^2)$ as a function of transverse momentum squared k_\perp^2 at Bjorken- x values of 10^{-1} , 10^{-2} , 10^{-3} , and 10^{-4} . The different curves are obtained from our loop-loop correlation model (LLCM), the Golec-Biernat and Wüsthoff (GBW) model [44], the derivative of the Glück, Reya, and Vogt (GRV) parametrization of $xG_p(x, Q^2)$ [51], and the Ivanov and Nikolaev (IN) approach [49].

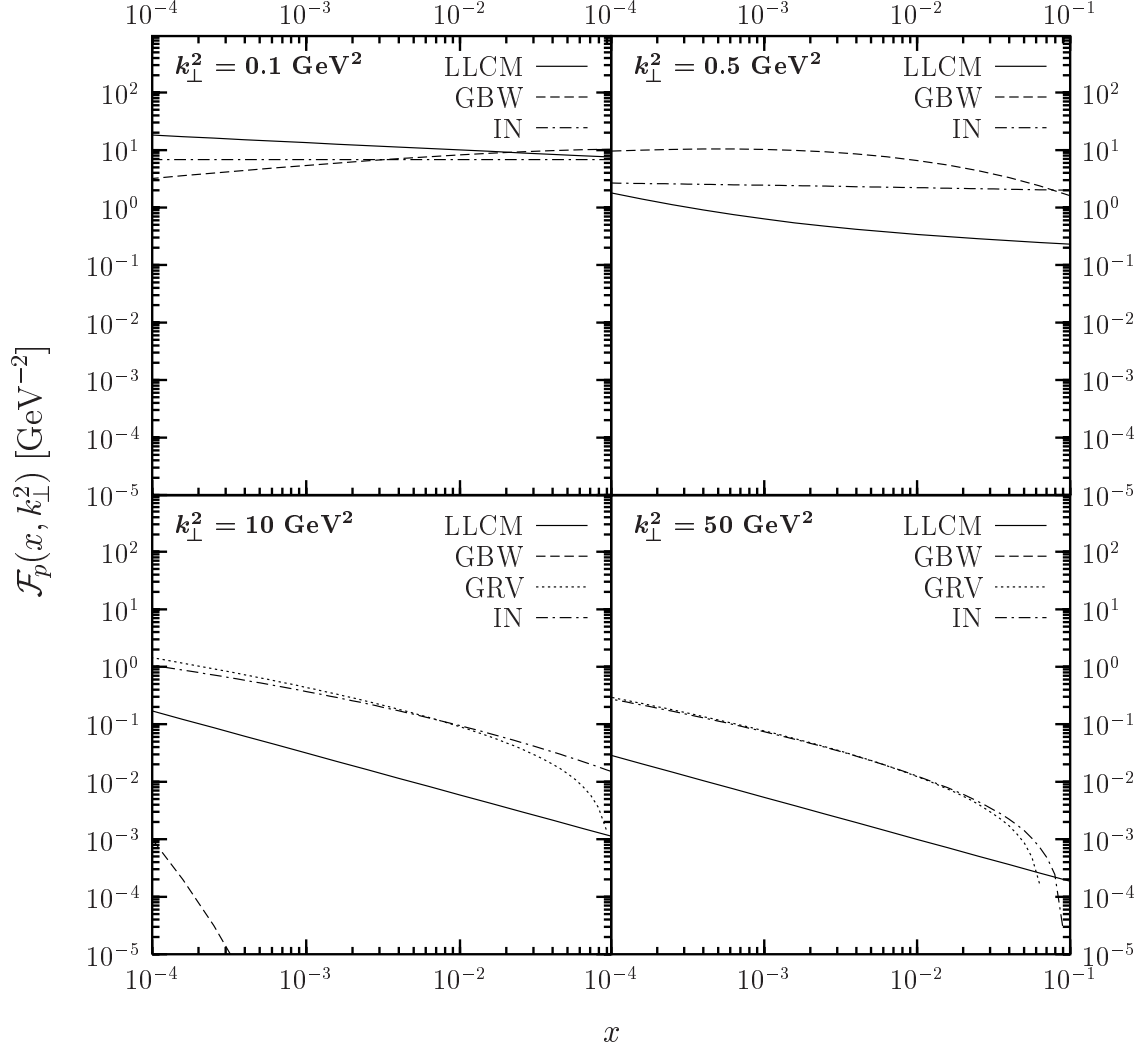


Figure 14: The unintegrated gluon distribution of the proton $\mathcal{F}_p(x, k_\perp^2)$ as a function of Bjorken- x at transverse momenta squared $k_\perp^2 = 0.1, 0.5, 10,$ and 50 GeV^2 . The different curves are obtained from our loop-loop correlation model (LLCM), the Golec-Biernat and Wüsthoff (GBW) model [44], the derivative of the Glück, Reya, and Vogt (GRV) parametrization of $xG_p(x, Q^2)$ [51], and the Ivanov and Nikolaev (IN) approach [49]. Note that the GRV parametrization is only available for $k_\perp^2 \geq 0.8 \text{ GeV}^2$. Moreover, the GBW result for $\mathcal{F}_p(x, k_\perp^2)$ is below 10^{-5} for $k_\perp^2 = 50 \text{ GeV}^2$.

In addition to the one-scale unintegrated gluon distributions, $\mathcal{F}(x, k_{\perp}^2)$, discussed in this work, there exist also two-scale unintegrated gluon distributions, $\mathcal{F}(x, k_{\perp}^2, \mu^2)$. In the CCFM evolution equation [24], this additional scale μ^2 is related to the maximum angle allowed in the gluon emission. Two-scale unintegrated gluon distributions are obtained in the approach of Blümlein [53], Jung and Salam [54], Kimber, Martin, and Ryskin [55], and in the linked dipole chain (LDC) model [56, 57]. A comparison of their results can be found in [57, 58] where also the one-scale unintegrated gluon distributions of Kwiecinski, Martin and Stasto [59], and Ryskin and Shabelski [60] are discussed.

7 Conclusions

We have investigated perturbative and non-perturbative QCD contributions to high-energy scattering in momentum space within the recently presented loop-loop correlation model [1]. The perturbative contribution has been described by two-gluon exchange and the non-perturbative contribution by the stochastic vacuum model of QCD which leads to confinement of the quark and antiquark in a dipole via a string of color fields. This QCD string gives important non-perturbative contributions to high-energy reactions and manifests itself in the linear increase of the total dipole-hadron cross section for large dipole sizes. A new structure different from perturbative two-gluon exchange has been found in the non-perturbative string-string interaction. A decomposition of the confining string into dipoles has allowed us to extract the microscopic structure of the unintegrated gluon distribution of hadrons and photons from the dipole-hadron and dipole-photon cross section via $|\vec{k}_{\perp}|$ -factorization.

The minimal surfaces used in our loop-loop correlation model [1] have allowed us to show for the first time the QCD structure of the non-perturbative contribution to the dipole-dipole scattering amplitude in momentum space. This contribution has two parts: The first part describes the non-perturbative interaction between the quarks and antiquarks of the two dipoles and has the structure known from perturbative two-gluon exchange [19, 20]. The second part describes the interaction between the strings of the two dipoles and has a new structure originating from the geometry of the strings. The string contribution, however, is negligible in the scattering of two small dipoles which is governed by perturbative physics.

The contribution of the confining string to the total dipole-hadron cross section $\sigma_{Dh}(x, |\vec{r}_D|)$ has been studied. For small dipole sizes, $|\vec{r}_D| \rightarrow 0$, the string contribution shows color transparency, $\sigma_{Dh}(x, |\vec{r}_D|) \propto r_D^2$, as known for the perturbative contribution. For large dipole sizes, $|\vec{r}_D| \gtrsim 0.5$ fm, the non-perturbative contribution increases

linearly with increasing dipole size, $\sigma_{Dh}(x, |\vec{r}_D|) \propto |\vec{r}_D|$, in contrast to the perturbative contribution which gives an $|\vec{r}_D|$ -independent dipole-hadron cross section. This linear increase is generated by the interaction of the string of the dipole with the hadron: the longer the string, the larger the geometric cross section with the hadron. String breaking, expected to stop the linear increase for $|\vec{r}_D| \gtrsim 1$ fm, is not obtained in our model working in the quenched approximation. In our model, $|\vec{k}_\perp|$ -factorization has been found to be valid also for the non-perturbative contribution to $\sigma_{Dh}(x, |\vec{r}_D|)$.

A very interesting feature of the string confining the quark and antiquark in the dipole has been found: A string of length $|\vec{r}_D|$ can be represented as an integral over stringless dipoles of sizes $\xi|\vec{r}_D|$ with $0 \leq \xi \leq 1$ and dipole number density $n(\xi) = 1/\xi^2$. A similar behavior has been observed for the perturbative wave function of a $q\bar{q}$ onium state in the large- N_c limit where the numerous emitted gluons are considered as dipoles [47, 48]. The decomposition of the string into stringless dipoles has allowed us to rewrite the string-hadron scattering process as an incoherent superposition of dipole-hadron scattering processes and to extract the unintegrated gluon distribution of hadrons and photons from our dipole-hadron and dipole-photon cross section via $|\vec{k}_\perp|$ -factorization.

We have shown explicitly the microscopic structure of the unintegrated gluon distribution in hadrons and photons. For small momenta $|\vec{k}_\perp|$, the unintegrated gluon distributions of protons, pions, and kaons $\mathcal{F}_h(x, k_\perp^2)$ are dominated by non-perturbative physics and behave as $S_h^2/|\vec{k}_\perp|$ where S_h denotes the hadron extension. The $1/|\vec{k}_\perp|$ -behavior reflects the linear increase of the total dipole-hadron cross section at large dipole sizes. The unintegrated gluon distributions of protons, pions, and kaons differ at small momenta because of their different extensions: $S_p = 0.86$ fm, $S_\pi = 0.607$ fm, and $S_K = 0.55$ fm. For large momenta, $|\vec{k}_\perp| \gtrsim 1$ GeV, the unintegrated gluon distributions of the hadrons are dominated by perturbative physics and show the $1/k_\perp^2$ -behavior induced by the gluon propagator. In the perturbative region of large momenta, the valence constituents are resolved and the dependence of the unintegrated gluon distribution on the hadron extension S_h vanishes. In contrast, the unintegrated gluon distribution of photons depends on the “photon size” controlled by the photon virtuality Q^2 for large $|\vec{k}_\perp|$. For very large $|\vec{k}_\perp|$, the unintegrated gluon distributions of hadrons and photons become parallel in line with the vanishing dependence on the specific form of the wave function.

The x -dependence of the unintegrated gluon distribution of hadrons and photons has been introduced phenomenologically into our model. Motivated by the successful description of many experimental data in our recent work [1], we have given a strong energy dependence to the perturbative contribution and a weak one to the non-perturbative contribution. Consequently, with decreasing x the perturbative

contribution increases much stronger than the non-perturbative contribution and extends into the small- $|\vec{k}_\perp|$ region. A similar hard-to-soft diffusion is observed also in the approach of Ivanov and Nikolaev [49] while a soft-to-hard diffusion is obtained in the approach of the color glass condensate [50]. Considering the integrated gluon distribution of the proton $xG_p(x, Q^2)$, our non-perturbative contribution dominates for $x \gtrsim 10^{-3}$ while the perturbative contribution becomes relevant for $x \lesssim 10^{-3}$ and generates the steep increase of $xG_p(x, Q^2)$ with decreasing x at fixed Q^2 . Also the rise of $xG_p(x, Q^2)$ with increasing Q^2 at fixed x results from the strong energy dependence of the perturbative contribution.

We have compared the unintegrated gluon distribution of the proton $\mathcal{F}_p(x, k_\perp^2)$ extracted from our loop-loop correlation model (LLCM) with those obtained from the saturation model of Golec-Biernat and Wüsthoff (GBW) [44], the derivative of the Glück, Reya, and Vogt (GRV) parametrization of $xG_p(x, Q^2)$ [51], and the approach of Ivanov and Nikolaev (IN) [49]. For $k_\perp^2 \rightarrow 0$, the unintegrated gluon distribution of GBW decreases as k_\perp^2 and the one of IN as k_\perp^4 in contrast to the $1/\sqrt{k_\perp^2}$ -decrease found in our model. In the perturbative region, the LLCM, GRV, and IN unintegrated gluon distributions become parallel for $x \lesssim 10^{-2}$ and drop as $1/k_\perp^2$ with increasing k_\perp^2 . This perturbative QCD behavior is not reproduced by the GBW unintegrated gluon distribution which decreases exponentially with increasing k_\perp^2 . The x -dependence of the considered unintegrated gluon distributions is weak in the non-perturbative region and becomes stronger as k_\perp^2 increases.

The unintegrated gluon distributions of hadrons and photons, $\mathcal{F}_h(x, k_\perp^2)$, extracted from our model can be used to compute, for example, dijet and vector meson production. So far, the unintegrated gluon distribution is obtained from the lowest order contribution to the T -matrix element and can only be used for $x \gtrsim 10^{-4}$. For smaller values of x , multiple gluonic exchanges become important and necessary to respect S -matrix unitarity constraints [1]. Thus, a formalism must be developed that allows to extract an unintegrated gluon distribution which takes into account multiple gluonic exchanges.

Acknowledgements

A. Shoshi and F. Steffen would like to thank C. Ewerz, H. Forkel, and A. Polleri for interesting discussions and Yu. Ivanov for his support in computational issues. This research was supported in part by the National Science Foundation under Grant No. PHY99-07449 and the Intas project “Nonperturbative QCD.”

A Hadron and Photon Wave Functions

The light-cone wave functions $\psi_i(z_i, \vec{r}_i)$ provide the distribution of transverse size and orientation \vec{r}_i and longitudinal quark momentum fraction z_i to the light-like Wegner-Wilson loops $W[C_i]$ that represent the scattering color-dipoles.

The Hadron Wave Function

In this work, mesons and baryons are assumed to have a quark-antiquark and quark-diquark valence structure, respectively. This allows us to model hadrons as color-dipoles. We use for the hadron wave function the phenomenological Gaussian Wirbel-Stech-Bauer ansatz [27]

$$\psi_h(z_i, \vec{r}_i) = \sqrt{\frac{z_i(1-z_i)}{2\pi S_h^2 N_h}} e^{-(z_i - \frac{1}{2})^2 / (4\Delta z_h^2)} e^{-|\vec{r}_i|^2 / (4S_h^2)}, \quad (\text{A.1})$$

where the constant N_h is fixed by the normalization of (A.1) to unity. The different hadrons considered — protons, pions, and kaons — are characterized by different values for Δz_h and S_h . The extension parameter S_h is a fit parameter that should resemble approximately the electromagnetic radius of the corresponding hadron while $\Delta z_h = w / (\sqrt{2} m_h)$ [27] is fixed by the hadron mass m_h and the value $w = 0.35 - 0.5 \text{ GeV}$ extracted from experimental data. We adopt the values of Δz_h and S_h from our previous work [1] as these values allow a good description of many experimental data: $\Delta z_p = 0.3$ and $S_p = 0.86 \text{ fm}$ for protons, $\Delta z_\pi = 2$ and $S_\pi = 0.607 \text{ fm}$ for pions, and $\Delta z_K = 0.57$ and $S_K = 0.55 \text{ fm}$ for kaons.

The Photon Wave Function

The photon wave function $\psi_\gamma(z_i, \vec{r}_i, Q^2)$ describes the fluctuation of a photon with virtuality Q^2 into a quark-antiquark pair with longitudinal quark momentum fraction z_i and spatial transverse size and orientation \vec{r}_i . The computation of the corresponding transition amplitude $\langle q\bar{q}(z_i, \vec{r}_i) | \gamma(Q^2) \rangle$ can be performed conveniently in light-cone perturbation theory [61] and leads to the following squared wave functions for transverse (T) and longitudinally (L) polarized photons [42]

$$|\psi_{\gamma_T^*}(z_i, \vec{r}_i, Q^2)|^2 = \frac{3\alpha}{2\pi^2} \sum_f e_f^2 \{ [z_i^2 + (1-z_i)^2] \epsilon_f^2 K_1^2(\epsilon_f |\vec{r}_i|) + m_f^2 K_0^2(\epsilon_f |\vec{r}_i|) \} \quad (\text{A.2})$$

$$|\psi_{\gamma_L^*}(z_i, \vec{r}_i, Q^2)|^2 = \frac{3\alpha}{2\pi^2} \sum_f e_f^2 \{ 4 Q^2 z_i^2 (1-z_i)^2 K_0^2(\epsilon_f |\vec{r}_i|) \}, \quad (\text{A.3})$$

where α is the fine-structure constant, e_f is the electric charge of the quark with flavor f , and K_0 and K_1 are the modified Bessel functions (McDonald functions). In the above expressions,

$$\epsilon_f^2 = z_i(1 - z_i) Q^2 + m_f^2 \quad (\text{A.4})$$

controls the transverse size(-distribution) of the emerging dipole, $|\vec{r}_i| \propto 1/\epsilon_f$, that depends on the quark flavor through the current quark mass m_f .

For small Q^2 , the perturbatively derived wave functions, (A.2) and (A.3), are not appropriate since the resulting large color-dipoles, i.e., $|\vec{r}_i| \propto 1/m_f \gg 1$ fm, should encounter non-perturbative effects such as confinement or chiral symmetry breaking. To take these effects into account, we introduce Q^2 -dependent quark masses, $m_f = m_f(Q^2)$, that interpolate between the current quarks at large Q^2 and the constituent quarks at small Q^2 [15]. In our recent work [1], we adjusted the running quark masses as follows

$$m_{u,d}(Q^2) = 0.178 \text{ GeV} \left(1 - \frac{Q^2}{Q_{u,d}^2}\right) \Theta(Q_{u,d}^2 - Q^2), \quad (\text{A.5})$$

$$m_s(Q^2) = 0.121 \text{ GeV} + 0.129 \text{ GeV} \left(1 - \frac{Q^2}{Q_s^2}\right) \Theta(Q_s^2 - Q^2), \quad (\text{A.6})$$

with the parameters $Q_{u,d}^2 = 1.05 \text{ GeV}^2$ and $Q_s^2 = 1.6 \text{ GeV}^2$. For the charm quark mass, we used a fixed value of

$$m_c = 1.25 \text{ GeV}. \quad (\text{A.7})$$

B The Non-Forward T -Matrix Element

In this appendix, we calculate the perturbative and non-confining contribution to the non-forward ($t \neq 0$) T -matrix element. We show explicitly that the non-forward T -matrix element depends on the parameters which control the z_i -distribution of the wave functions. These parameter are essential for a good description of differential elastic cross sections and the slope parameter as shown in our recent work [1].

The confining contribution to the non-forward ($t \neq 0$) T -matrix element is not presented. It is much more complicated since some of the integrations cannot be performed analytically. Nevertheless, we find numerically that it shows the same features concerning the z_i -distributions as the perturbative and non-confining contributions.

The perturbative contribution to the non-forward T -matrix element in the small- χ limit (2.24),

$$T^P(s_0, t) = \frac{2is_0}{9} \int d^2b_\perp e^{i\vec{q}_\perp \vec{b}_\perp} \int dz_1 d^2r_1 \int dz_2 d^2r_2 |\psi_1(z_1, \vec{r}_1)|^2 |\psi_2(z_2, \vec{r}_2)|^2 (\chi^P)^2, \quad (\text{B.1})$$

reduces upon integration over the impact parameter $|\vec{b}_\perp|$ to

$$\begin{aligned} T^P(s_0, t) &= \frac{32is_0}{9} \int d^2k_\perp \alpha_s(k_\perp^2) i\tilde{D}'^{(2)}(k_\perp^2) \alpha_s((\vec{k}_\perp + \vec{q}_\perp)^2) i\tilde{D}'^{(2)}((\vec{k}_\perp + \vec{q}_\perp)^2) \\ &\times \int_0^1 dz_1 \int_0^1 dz_2 \left[H_1(z_1^2 q_\perp^2) - H_1((z_1 \vec{q}_\perp + \vec{k}_\perp)^2) \right] \left[H_2(z_2^2 q_\perp^2) - H_2((z_2 \vec{q}_\perp + \vec{k}_\perp)^2) \right] \end{aligned} \quad (\text{B.2})$$

with

$$H_i((z_i \vec{q}_\perp + \vec{k}_\perp)^2) := \int d^2r_i |\psi_i(z_i, \vec{r}_i)|^2 e^{i\vec{r}_i \cdot (z_i \vec{q}_\perp + \vec{k}_\perp)}. \quad (\text{B.3})$$

and $|\psi_i(z_i, \vec{r}_i)|^2$ denoting hadron or photon wave functions.

The non-confining contribution to the non-forward T -matrix element in the small- χ limit (2.24),

$$T_{nc}^{NP}(s_0, t) = \frac{2is_0}{9} \int d^2b_\perp e^{i\vec{q}_\perp \vec{b}_\perp} \int dz_1 d^2r_1 \int dz_2 d^2r_2 |\psi_1(z_1, \vec{r}_1)|^2 |\psi_2(z_2, \vec{r}_2)|^2 (\chi_{nc}^{NP})^2, \quad (\text{B.4})$$

becomes analogously

$$\begin{aligned} T_{nc}^{NP}(s_0, t) &= \frac{8is_0}{9} \left(\frac{\pi^2 G_2 (1 - \kappa)}{24} \right)^2 \int \frac{d^2k_\perp}{(2\pi)^2} i\tilde{D}'^{(2)}(k_\perp^2) i\tilde{D}'^{(2)}((\vec{k}_\perp + \vec{q}_\perp)^2) \\ &\times \int_0^1 dz_1 \int_0^1 dz_2 \left[H_1(z_1^2 q_\perp^2) - H_1((z_1 \vec{q}_\perp + \vec{k}_\perp)^2) \right] \left[H_2(z_2^2 q_\perp^2) - H_2((z_2 \vec{q}_\perp + \vec{k}_\perp)^2) \right] \end{aligned} \quad (\text{B.5})$$

with $H_{1,2}$ defined in (B.3).

For $t = -q_\perp^2 \neq 0$, both contributions (B.2) and (B.5) depend on the shape of the z_i -distribution of the wave function, i.e., for the Gaussian hadron wave function (A.1), the contributions depend on the width Δz_h . This Δz_h -dependence is transferred to the differential elastic cross section

$$\frac{d\sigma^{el}}{dt}(s, t) = \frac{1}{16\pi s^2} |T(s, t)|^2 \quad (\text{B.6})$$

and its local slope

$$B(s, t) = \frac{d}{dt} \left(\ln \left[\frac{d\sigma^{el}}{dt}(s, t) \right] \right). \quad (\text{B.7})$$

At $t = 0$, the dependence on the shape of the z_i -distribution of the wave functions disappears because of the normalization of the z_i -distribution as can be seen immediately from (B.3). Therefore, in our model the total cross sections – related via the optical theorem to the forward ($t = 0$) T -matrix element – do not depend on the parameter that characterize the z_i -distribution of the wave function.

References

- [1] A. I. Shoshi, F. D. Steffen and H. J. Pirner, “S-Matrix Unitarity, Impact Parameter Profiles, Gluon Saturation and High-Energy Scattering,” hep-ph/0202012; Nucl. Phys. A in press.
- [2] O. Nachtmann, Annals Phys. **209** (1991) 436.
- [3] O. Nachtmann, in “Perturbative and Nonperturbative Aspects of Quantum Field Theory,” edited by H. Latal and W Schweiger (Springer Verlag, Berlin, Heidelberg 1997) [hep-ph/9609365].
- [4] A. Krämer and H. G. Dosch, Phys. Lett. B **252** (1990) 669.
- [5] H. G. Dosch, E. Ferreira and A. Krämer, Phys. Rev. D **50** (1994) 1992.
- [6] H. G. Dosch, in “Hadron Physics 96,” edited by E. Ferreira et al., (World Scientific, Singapore 1997).
- [7] H. G. Dosch, Phys. Lett. B **190** (1987) 177;
H. G. Dosch and Y. A. Simonov, Phys. Lett. B **205** (1988) 339;
Y. A. Simonov, Nucl. Phys. B **307** (1988) 512.
- [8] E. R. Berger and O. Nachtmann, Eur. Phys. J. C **7** (1999) 459.
- [9] L. Del Debbio, A. Di Giacomo and Y. A. Simonov, Phys. Lett. B **332** (1994) 111.
- [10] M. Rueter and H. G. Dosch, Z. Phys. C **66** (1995) 245.
- [11] A. I. Shoshi, F. D. Steffen, H. G. Dosch, and H. J. Pirner, HD-THEP-02-22 (2002).
- [12] N. E. Bralic, Phys. Rev. D **22** (1980) 3090;
P. M. Fishbane, S. Gasiorowicz and P. Kaus, Phys. Rev. D **24** (1981) 2324;
L. Diosi, Phys. Rev. D **27** (1983) 2552;
Y. A. Simonov, Sov. J. Nucl. Phys. **48** (1988) 878.

- [13] M. Rueter and H. G. Dosch, Phys. Lett. B **380** (1996) 177;
M. Rueter and H. G. Dosch, Phys. Rev. D **57** (1998) 4097;
G. Kulzinger, H. G. Dosch and H. J. Pirner, Eur. Phys. J. C **7** (1999) 73.
- [14] H. G. Dosch, T. Gousset, G. Kulzinger and H. J. Pirner, Phys. Rev. D **55** (1997) 2602.
- [15] H. G. Dosch, T. Gousset and H. J. Pirner, Phys. Rev. D **57** (1998) 1666.
- [16] M. Rueter, Eur. Phys. J. C **7** (1999) 233.
- [17] U. D'Alesio, A. Metz and H. J. Pirner, Eur. Phys. J. C **9** (1999) 601.
- [18] H. G. Dosch, O. Nachtmann, T. Paulus and S. Weinstock, Eur. Phys. J. C **21** (2001) 339.
- [19] F. E. Low, Phys. Rev. D **12** (1975) 163;
S. Nussinov, Phys. Rev. Lett. **34** (1975) 1286.
- [20] J. F. Gunion and D. E. Soper, Phys. Rev. D **15** (1977) 2617.
- [21] N. N. Nikolaev and B. G. Zakharov, Phys. Lett. B **332** (1994) 177;
A. Szczurek, N. N. Nikolaev, W. Schafer and J. Speth, Phys. Lett. B **500** (2001) 254.
- [22] J. Nemchik, N. N. Nikolaev, E. Predazzi, B. G. Zakharov and V. R. Zoller, J. Exp. Theor. Phys. **86** (1998) 1054.
- [23] E. A. Kuraev, L. N. Lipatov and V. S. Fadin, Sov. Phys. JETP **45** (1977) 199;
I. I. Balitsky and L. N. Lipatov, Sov. J. Nucl. Phys. **28** (1978) 822.
- [24] M. Ciafaloni, Nucl. Phys. B **296** (1988) 49;
S. Catani, F. Fiorani and G. Marchesini, Phys. Lett. B **234** (1990) 339.
- [25] V. N. Gribov and L. N. Lipatov, Yad. Fiz. **15** (1972) 781;
L. N. Lipatov, Sov. J. Nucl. Phys. **20** (1975) 94;
G. Altarelli and G. Parisi, Nucl. Phys. B **126** (1977) 298;
Y. L. Dokshitzer, Sov. Phys. JETP **46** (1977) 641.
- [26] F. J. Wegner, J. Math. Phys. **12** (1971) 2259;
K. G. Wilson, Phys. Rev. D **10** (1974) 2445.
- [27] M. Wirbel, B. Stech and M. Bauer, Z. Phys. C **29** (1985) 637.
- [28] A. Donnachie and P. V. Landshoff, Phys. Lett. B **437** (1998) 408; "New data and the hard pomeron," hep-ph/0105088.

- [29] J. R. Forshaw, G. Kerley and G. Shaw, Phys. Rev. D **60** (1999) 074012.
- [30] A. Donnachie and H. G. Dosch, Phys. Rev. D **65** (2002) 014019.
- [31] A. Di Giacomo and E. Meggiolaro, “On the dependence of the gauge-invariant field-strength correlators in QCD on the shape of the Schwinger string,” hep-lat/0203012.
- [32] A. Di Giacomo and H. Panagopoulos, Phys. Lett. B **285** (1992) 133;
A. Di Giacomo, E. Meggiolaro and H. Panagopoulos, Nucl. Phys. B **483** (1997) 371;
M. D’Elia, A. Di Giacomo and E. Meggiolaro, Phys. Lett. B **408** (1997) 315;
G. S. Bali, N. Brambilla and A. Vairo, Phys. Lett. B **421** (1998) 265.
- [33] E. Meggiolaro, Phys. Lett. B **451** (1999) 414.
- [34] W. Magnus, F. Oberhettinger and R. P. Soni, “Formulas and Theorems for the Special Functions of Mathematical Physics,” 3rd edition, edited by B. Eckmann and B. L. van der Werden (Springer Verlag, Berlin, Heidelberg, New York 1996).
- [35] S. Wolfram, “The Mathematica Book,” 4th edition, edited by G. Beck, J. Grohens and J. Walsh (Wolfram Research Inc., Cambridge University Press, 1999).
- [36] K. Golec-Biernat and M. Wüsthoff, Phys. Rev. D **59** (1999) 014017.
- [37] H. Abramowicz and A. Caldwell, Rev. Mod. Phys. **71** (1999) 1275;
J. Breitweg *et al.* [ZEUS Collaboration], Eur. Phys. J. C **7** (1999) 609;
C. Adloff *et al.* [H1 Collaboration], Eur. Phys. J. C **21** (2001) 33.
- [38] A. I. Shoshi, F. D. Steffen and H. J. Pirner, “Gluon Saturation and S-Matrix Unitarity,” hep-ph/0205343.
- [39] E. Laermann, C. DeTar, O. Kaczmarek and F. Karsch, Nucl. Phys. Proc. Suppl. **73** (1999) 447.
- [40] G. S. Bali, Phys. Rept. **343** (2001) 1.
- [41] S. Catani, M. Ciafaloni and F. Hautmann, Phys. Lett. B **242** (1990) 97; Nucl. Phys. B **366** (1991) 135.
- [42] N. N. Nikolaev and B. G. Zakharov, Z. Phys. C **49** (1991) 607.
- [43] N. N. Nikolaev and B. G. Zakharov, Phys. Lett. B **332** (1994) 184.
- [44] K. Golec-Biernat and M. Wüsthoff, Phys. Rev. D **60** (1999) 114023.

- [45] B. Blaettel, G. Baym, L. L. Frankfurt and M. Strikman, Phys. Rev. Lett. **70** (1993) 896.
- [46] N. N. Nikolaev and B. G. Zakharov, Phys. Lett. B **332** (1994) 184;
L. Frankfurt, W. Koepf and M. Strikman, Phys. Rev. D **54** (1996) 3194.
- [47] A. H. Mueller, Nucl. Phys. B **415** (1994) 373.
- [48] A. H. Mueller and B. Patel, Nucl. Phys. B **425** (1994) 471.
- [49] I. P. Ivanov and N. N. Nikolaev, Phys. Rev. D **65** (2002) 054004.
- [50] E. Iancu, A. Leonidov and L. McLerran, “The Colour Glass Condensate: An Introduction,” hep-ph/0202270.
- [51] M. Glück, E. Reya and A. Vogt, Eur. Phys. J. C **5** (1998) 461.
- [52] J. Bartels, K. Golec-Biernat and H. Kowalski, Phys. Rev. D **66** (2002) 014001.
- [53] J. Blümlein, “On the k_{\perp} dependent gluon density of the proton,” hep-ph/9506403.
- [54] H. Jung, “CCFM prediction on forward jets and F2: Parton level predictions and a new hadron level Monte Carlo generator CASCADE,” hep-ph/9908497;
H. Jung and G. P. Salam, Eur. Phys. J. C **19** (2001) 351.
- [55] M. A. Kimber, A. D. Martin and M. G. Ryskin, Phys. Rev. D **63** (2001) 114027.
- [56] B. Andersson, G. Gustafson and J. Samuelsson, Nucl. Phys. B **467** (1996) 443;
B. Andersson, G. Gustafson and H. Kharraziha, Phys. Rev. D **57** (1998) 5543.
- [57] G. Gustafson, L. Lonnblad and G. Miu, “Gluon Distribution Functions in the k_{\perp} -Factorization Approach,” hep-ph/0206195.
- [58] B. Anderson *et al.* [Small x Collaboration], “Small x Phenomenology: Summary and Status,” hep-ph/0204115.
- [59] J. Kwiecinski, A. D. Martin and A. M. Stasto, Phys. Rev. D **56** (1997) 3991.
- [60] M. G. Ryskin and Y. M. Shabelski, Z. Phys. C **66** (1995) 151.
- [61] J. D. Bjorken, J. B. Kogut and D. E. Soper, Phys. Rev. D **3** (1971) 1382;
G. P. Lepage and S. J. Brodsky, Phys. Rev. D **22** (1980) 2157.